Received: 31 July 2024 | Revised: 21 March 2025 | Accepted: 6 April 2025

DOI: 10.1111/joa.14262

Journal of Anatomy | ANATOMICAL SOCIETY WILEY

ORIGINAL ARTICLE

Osteohistological analysis of metatarsals reveals new information on pathology and life history of troodontids from the Campanian Dinosaur Park Formation, Alberta, Canada

Christiana W. Garros[1] | Mark J. Powers[1] | Aaron D. Dyer[2,3] | Philip J. Currie[1]

[1]Department of Biological Sciences, University of Alberta, Edmonton, Alberta, Canada

[2]Department of Ecology and Evolutionary Biology, University of Toronto, Toronto, Ontario, Canada

[3]Department of Natural History, Royal Ontario Museum, Toronto, Ontario, Canada

Correspondence
Christiana W. Garros, Department of Biological Sciences, University of Alberta, CW-405 Biological Sciences Building, Edmonton AB T6G 2E9, Canada.
Email: garros@ualberta.ca

Funding information
Natural Sciences and Engineering Research Council of Canada

Abstract

Troodontidae is a family of small-bodied theropods known predominantly from Asia but are comparatively scarce in North America. In the Dinosaur Park Formation (DPF) of Alberta, Canada, they are known predominantly from isolated material, precluding taxonomic and ontogenetic precision for this clade. Previously never sampled histologically within the DPF, here we attempt to fill in gaps in our knowledge about the life histories of the clade in this formation by histologically surveying metatarsals, which are among the most abundant and identifiable troodontid elements in the DPF. We sampled 11 metatarsals (three metatarsal IIs, three metatarsal IIIs and five metatarsal IVs) of varying sizes and included three pathological individuals to describe the microanatomy of both healthy and pathological metatarsals, determine the ontogenetic status of each element and graph their pattern of growth. Osteohistology reveals that troodontid metatarsals grew and remodelled asymmetrically within the cortex, ceasing growth and remodelling primarily along articular surfaces and entheses. Pathological individuals ranged from displaying features of response to localised stress (chronic callus formation and avulsion/chip fracture) to extreme modification in response to trauma and inflammation at the distal joint. Only the latter appeared to be related to overall growth, suggesting the condition either developed early and stunted growth or another underlying cause was responsible for both the stunted growth and the resulting pathological features observed. Overall, tracking the growth of the specimens reveals that there are at least two growth trajectories within the DPF differentiated by the timing of major growth spurts and growth plateaus. Whether this represents sexual dimorphism, taxonomic diversity, or another form of variation warrants further investigation.

KEYWORDS
arctometatarsus, fracture, growth, histology, inflammation, metatarsals, ontogeny, paleopathology, remodelling, stress, trauma, Troodontidae

1 | INTRODUCTION

Troodontidae is a family of theropods that lived from the Late Jurassic to the Late Cretaceous and is characterised by a light build, long legs, large eyes and a large braincase relative to their size (Currie, 1985; Hartman et al., 2019; Norell et al., 2009; Tsuihiji et al., 2014). Generally small bodied, they ranged in size from less than 1 m (*Mei long* in Xu & Norell, 2004) to an estimated 2 m or more (*Stenonychosaurus inequalis* in Russell & Séguin, 1982 and *Zanabazar junior* in Norell et al., 2009). However, large trackways in China and large teeth in Alaska have suggested that larger forms may have existed (Fiorillo, 2008; Horner et al., 2001; Prondvai et al., 2018; Xing et al., 2024). Their bird-like qualities and small body size have made troodontids attractive candidates for histological work aimed at understanding the evolution of dinosaur life histories. So far, nine species have been histologically assessed, approximately 35% of known species (Erickson et al., 2009; Gao et al., 2012; Martin et al., 2023, 2024; Prondvai et al., 2018; Sellés et al., 2021; Shen, Lü, et al., 2017; Shen, Zhao, et al., 2017; Varricchio, 1993; Xu et al., 2008, 2012; Zanno et al., 2011). This body of osteohistological work demonstrates that troodontids had active metabolisms and grew quickly, with some smaller forms attaining adult size in an estimated two years, whereas larger forms could take four to six (Gao et al., 2012; Varricchio, 1993; Zanno et al., 2011). Despite difficulty in pinpointing the precise onset of sexual maturity, histology on an undescribed brooding troodontid specimen, as well as other brooding small-bodied theropods, suggests that it occurred prior to reaching somatic maturity, unlike extant birds (Erickson et al., 2007). Histology has also been used to tackle taxonomic and ontogenetic uncertainties, such as determining if small specimens are simply juveniles of a larger species or understanding the development of important characters (Funston et al., 2020; Gao et al., 2012).

Most of the histologically studied species thus far are from Asia, which is unsurprising considering most of the known diversity of the family and the most complete specimens are from there (Lü et al. 2010; Norell et al., 2009; Tsuihiji et al., 2014). Material from North America, however, has remained comparatively scarce (Currie, 1985; Evans et al., 2017; Russell, 1969; Sternberg, 1932; van der Reest & Currie, 2017; Zanno et al., 2011). Furthermore, only *Troodon* sp. from the Campanian Two Medicine and Judith River Formations of Montana and *Talos sampsoni* from the Campanian Kaiparowits Formation of Utah have been studied histologically (Erickson et al., 2009; Horner et al., 2001; Varricchio, 1993; Varricchio et al., 2008; Zanno et al., 2011). As a result, our understanding of troodontid diversity and life histories in North America is still relatively poor and more labile.

The Campanian Dinosaur Park Formation (DPF), Alberta, Canada, is well known for its dinosaur richness and diversity, but small-bodied dinosaurs (<60 kg) are relatively underrepresented, attributed to a preservation bias associated with alluvial/paralic sedimentary deposits (Brown et al., 2013, 2022). Thus, troodontid material from the DPF is largely composed of isolated bones, making taxonomic diversity in the formation difficult to ascertain (Cullen, Zanno, et al., 2021). Without good material and a solid understanding of the taxonomic relationships within an ecosystem, our understanding of the life histories and behaviours of individuals within species is also limited. However, histological sampling of multiple isolated specimens can be a powerful tool for assessing troodontid diversity in the DPF. By examining what growth trajectories are present, we can assess whether there were multiple taxon-specific body sizes, as was done previously with Caenagnathidae by Funston et al. (2020). Additionally, DPF specimens can be compared to other troodontids to get a better overall picture of the life history of the troodontids of the DPF, which have never been histologically studied before.

Although studies comparing the histology of multiple troodontid taxa and/or elements with each other to study evolution have been done previously, there are some important caveats to consider (Martin et al., 2024). The histology of different bones within an individual can vary significantly in estimated growth rates and patterns of both number and spacing in lines of arrested growth (LAGs) and/or annuli, and other variables such as osteocyte lacunae density. For example, in ornithomimids, caenagnathids and troodontids, fibulae have been found to have an extra LAG compared to other elements of the hindlimb, and certain bones appear to grow quicker relative to others (Cullen et al., 2014; Cullen, Simon, et al., 2021; Martin et al., 2023; Zanno et al., 2011). This also has implications for using circumference and length of long bones for estimating body size as different bones have been shown histologically to scale differently as they grow (Cullen, Brown, et al., 2021). The spacing between a set of growth marks can vary throughout the cortex, which can also add an element of uncertainty when only partial sections are taken from bones instead of a complete cross section, particularly when using large weight-bearing limb bones (the gold-standard for reconstructing growth) (Cullen et al., 2020). Therefore, any individual histological section should never be considered absolute in terms of the information it conveys about a taxon or even an individual. Comparisons between individuals, both intra- and interspecifically, must be done carefully and always considering which bone was sampled, where it was sampled, how complete the histological section is and how growth rate was measured.

Troodontid metatarsals are distinct, diagnosable and among the most abundant and well-preserved troodontid elements found in the DPF. Their abundance, weight-bearing nature, excellent 3D preservation, identifiability (even when fragmentary) and small size make them good candidates for a histological survey within the context of the DPF in lieu of sufficient femora and tibiae. Like dromaeosaurids, the troodontid pes bore an elongated sickle claw on digit II that was held off the ground (Russell, 1969; Zanno et al., 2011). However, the articulation in the digit differs substantially between the two taxa, with dromaeosaurids having a much more extreme ginglymoid (spindle-shaped) articulation between phalanx II-1 and metatarsal II (MTII), whereas troodontids had a more rounded cup-like proximal articular surface on phalanx II-1 (Fowler et al., 2011). Additionally, troodontid metatarsals were typically much longer proportionally and express the arctometatarsalian condition, in which metatarsal III

(MTIII) tapers proximally into a thin splint and is compressed by the outer two metatarsals: (MTII) and metatarsal IV (MTIV) (Holtz, 1995) (Figure 1). This forms a very compact and efficient structure for greater cursoriality. Because of the retention of a sickle claw, however, the arctometatarsus in troodontids does not have the typical appearance wherein MTII and MTIV are more or less equal in width, and both participate in weight bearing. Instead, MTII is laterally compressed and reduced, while MTIV is more robust (Holtz, 1995; Zanno et al., 2011).

This unique morphology falls somewhere in between the extremes of the cursoriality seen in ornithomimids and the specialised larger raptorial claw in dromaeosaurs and raises questions about the articulation and soft tissue structures involved in the structure (Rhodes et al., 2021). Intermediate morphologies of this kind could suggest a more generalist life habit, a hypothesis supported by biogeochemical data of troodontid teeth (Cullen & Cousens, 2024). Additionally, preliminary surveys of museum specimens from the DPF have revealed pathologies affecting a higher proportion of troodontid metatarsals compared to other similarly sized DPF theropods (Garros et al. 2022; conference abstract). Paleopathology and histopathology can provide a unique lens with which to study these questions by examining moments in an individual's life and the response to such events. Furthermore, while pathologies have been reported in troodontids in other elements (pedal phalanx in Zanno et al., 2011; vertebra in Wang et al., 2022), none have been studied histologically. Thus, pathological specimens were included in the present study alongside healthy ones to compare their growth and signs of stress in addition to diagnosing their conditions.

2 | MATERIALS

All specimens were selected from the collections of the Royal Tyrrell Museum of Palaeontology (TMP) based on their identifications as metatarsals referable to the family Troodontidae from the DPF. This was determined based on the unique morphology of troodontid

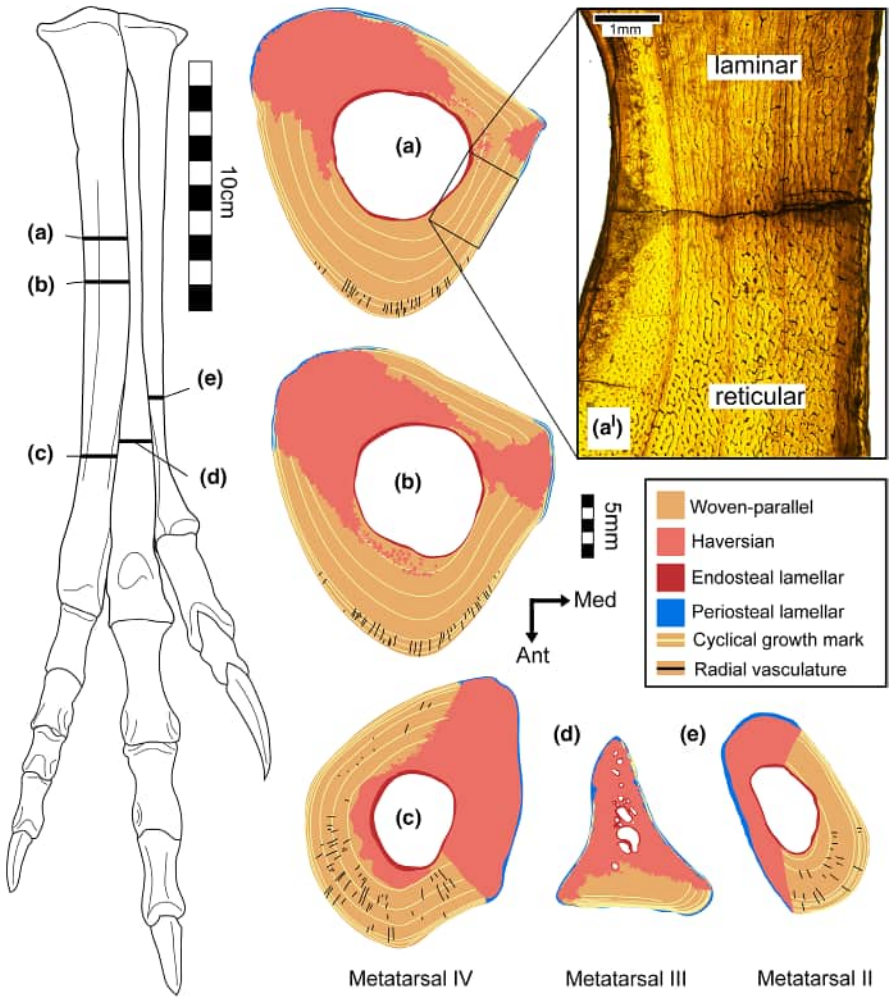

FIGURE 1 Osteohistology of troodontid metatarsals based on specimens from the Dinosaur Park Formation. (a–c) Sections of metatarsal IV (MTIV) based on TMP2003.012.0065. (d) Metatarsal III (MTIII) based on TMP1997.0133.0008. (e) Metatarsal IV (MTII) based on TMP1999.055.0118. (a^{l}) Inset illustrating two examples of the different types of woven-parallel complexes that can be found in the cortex of troodontid metatarsals.

metatarsals (Fowler et al., 2011; Holtz, 1995; Sternberg, 1932; Wilson & Currie, 1985; Zanno et al., 2011). Specimens of various sizes were chosen to capture a more complete growth series and to examine different growth patterns, if present at different stages of growth. Specimens showing clear pathologies were selected in addition to those with few and relatively subtle pathologies to examine the potential differences in growth patterns and rates. These inclusions were influenced by the rather high abundance of pathologies within these elements of troodontids, despite them being a small-bodied clade (Garros et al., 2022; conference abstract). Relatively complete, disarticulated elements were preferred, as they contained more information regarding size, as well as comparison between metatarsals of a single individual in the case of associated specimens (TMP1992.036.0720, TMP1999.055.0118). Any identifiable element with overlapping portions of the shaft was considered. In total, there were nine individuals selected, two of which had two associated elements for a total of 11 metatarsals: three MTIIs, three MTIIIs and five MTIVs (Table 1).

3 | METHODS

3.1 | Histological sampling

Prior to histological sampling, photogrammetry models were produced for all specimens with a customised Optima Surface Scanner housed in the Sullivan Lab at the University of Alberta and processed in FlexScan3D v.3.3 software. Histological sampling methods followed Padian and Lamm (2013). Areas of interest were removed from larger specimens (e.g. removing a section of the midshaft) to avoid unnecessary polyester resin immersion. Smaller specimens were embedded as whole samples. Castolite AC polyester resin was used to embed all specimens, which were immediately placed in a vacuum chamber to allow the resin to penetrate fractures and vessels. Specimens embedded in cured resin blocks were then sectioned with a Buehler Isomet 1000 low wafer saw blade. Cut surfaces and plexiglass microscope slides were polished with a water slurry of 600-grit silicon carbide abrasive powder. These were then mounted together with cyanoacrylate. Mounted blocks were then sectioned 0.7 mm from the surface of the plexiglass to produce a wafer. The thin wafers were then handground with subsequent 600 and 1000 grit silicon carbide slurries and given a final polish with a microfibre cloth. Thin sections were examined with a Nikon Eclipse E600 POL polarising microscope. High-resolution images were captured with a Nikon DS-Fi3 camera and processed in NIS Elements-D imaging software.

As previous studies have highlighted, some histological features such as LAGs can vary between different bones within a specimen, making comparisons between individuals and/or taxa from isolated elements difficult (Cullen et al., 2014). To mitigate this, only sections taken from the same region of the same element (e.g. the same spot on the shaft for multiple MTIVs) were compared between individuals for tracking growth. Sections were taken as close to the midshaft as possible, as per long-bone histology standards, but priority was given to sectioning in regions that permitted the comparison of the largest number of elements possible. Thus, sections were taken from shaft regions that permitted the greatest number of overlaps between individuals in addition to the sections that were taken for pathological analysis.

3.2 | Histological nomenclature

Categories and terminology for osteohistological features predominantly follow Francillon-Vieillot et al. (1990) and de Ricqlès (1980) with a few exceptions. First is the use of internal fundamental system (IFS) and external fundamental system (EFS) to refer to the avascular parallel-fibered or lamellar bone that can be found bordering the endosteum and periosteum, respectively (de Buffrénil & Quilhac, 2021; Enlow, 1963). These features are also known as the inner circumferential layer (ICL) and outer circumferential layer (OCL), but we have opted to use IFS and EFS given their prevalence in the dinosaur histology literature (de Buffrénil & Quilhac, 2021). Secondly, we have opted to use the term woven-parallel complexes/bone (WPCs) instead of fibrolamellar bone as proposed by de Buffrénil and Quilhac (2021) and Prondvai et al. (2014) for its greater descriptive power and accuracy. Vascular orientation (longitudinal, plexiform, radial, reticular) was described relative to the plane of section, all of which were transverse. Another important distinction is that of LAGs versus annuli. Both are types of cyclical growth marks (CGMs): circumferential rings in periosteal-derived cortical tissue indicative of a periodical drop in growth rate but differ in appearance (de Buffrénil & Quilhac, 2021). When these appear in the form of conspicuous bands of slow-growing parallel-fibered or lamellar bone, they are referred to as *annuli*, and they are attributed to growth that has slowed considerably but has not ceased. If the growth rate slows enough, it may temporarily halt, depositing a dark circumferential line called an LAG (de Buffrénil & Quilhac, 2021). Both occur from similar processes and thus both are used for tracking growth. Both terms are used here, but for simplicity, when discussing growth curve measurements and labelling figures, 'CGMs' will be used to refer to both types.

3.3 | Assessment of ontogenetic stages

Previous studies concerned with growth in troodontids (and dinosaurs in general) have used various qualitative markers to classify specimens based on age (Gao et al., 2012; Shen, Lü, et al., 2017; Shen, Zhao, et al., 2017; Xu et al., 2012; Zanno et al., 2011). However, lack of standardisation in terminology and differing interpretations of structures have created some confusion (Martin et al., 2024). For example, the terms 'subadult' and 'sexually mature' have been used interchangeably to refer to specimens with an IFS but no fully developed EFS, despite those terms referring

TABLE 1 Summary of Dinosaur Park Formation troodontid metatarsals histologically analysed and the presence of ontogenetically informative features.

Specimen	Element	Section #	Circumference (mm) (including pathologic regions)	Area (mm^2) (including pathologic regions)	Number of visible cyclical growth marks	Plateau in zone thickness?	Sudden change in cortical tissue, from endosteum to periosteum?	Secondary osteons?	EFS?	Interpretation
TMP1994.012.0884	MTII	94II-1	36.260	87.385	4	No	Yes	Yes	No	Juvenile
		94II-2	35.632	88.941	NA	No	No	Yes	No	
TMP1999.055.0118	MTII	99II-1	42.881	122.737	7	Yes	No	Yes	Regional	Late subadult–adult
	MTIV	99IV-1	71.656	381.967	7	Yes	No	Yes	Regional	
		99IV-2	76.602	427.012	NA	Yes	No	Yes	Regional	
TMP1992.036.0720*	MTII	92II-1	39.267	95.602	9	Yes	Yes	Yes	Yes	Adult
		92II-2	39.673	93.867	10	Yes	Yes	Yes	Yes	
	MTIV	92IV-1	72.705	356.002	NA	Yes	Yes	Yes	Yes	
		92IV-2	72.260	390.013	10	Yes	No	Yes	Regional	
		92IV-3	78.682	457.127	10	Yes	No	Yes	Regional	
TMP1997.0133.0008	MTIII	97III	43.841	88.685	?	Yes	Yes	Yes	Regional	Adult?
TMP1998.068.0090	MTIII	98III	39.457	106.192	1–2	No	Yes	Yes	No	Juvenile
TMP2005.049.0015	MTIII	05III	31.125	52.932	?	?	Yes	Yes	?	Juvenile?
TMP1967.020.0026*	MTIV	67IV-1	68.48	326.46	7	Yes	Yes	Yes	Regional	Late subadult–adult
		67IV-2	70.490	348.163	8	Yes	Yes	Yes	Yes	
TMP2003.012.0065	MTIV	03IV-1	61.666	275.964	7	Yes	No	Yes	Regional	Subadult
		03IV-2	73.883	395.937	NA	Yes	No	Yes	No	
		03IV-3	74.283	394.163	7	Yes	No	Yes	Regional	
TMP2005.049.0086*	MTIV	05IV-1	67.404	322.401	7	Yes	Yes	Yes	Regional	Late subadult
		05IV-2	77.543	413.503	7	Yes	Yes	Yes	Regional	
		05IV-3	78.973	406.233	NA	Yes	Yes	Yes	Regional	

Note: Only visible cyclical growth marks are included in this table, so those that were estimated using retrocalculation are not included. Note that specimens denoted with an asterisk were pathologic and thus warrant special consideration.

to different physiological characteristics (Shen, Lü, et al., 2017; Shen, Zhao, et al., 2017; Xu et al., 2008). Because of this confusion, Martin et al. (2024) have proposed a standard set of characteristics for classifying histological specimens as juvenile, subadult, or adult, which we follow here.

3.3.1 | Extent of zonation

Zones describe regions of the cortex from endosteum to periosteum demarcated by CGMs (LAGs and annuli). A lack of zones, and therefore a lack of visible CGMs, is considered a juvenile characteristic (Horner et al., 2001; Martin et al., 2024).

3.3.2 | Changes in cortical tissue and/or vascularity

As bone matures and the cortex expands outwards from the periosteum, it may change in microstructure (Prondvai et al., 2014). This includes changes in the type of intercellular matrix (e.g. woven-parallel to parallel-fibered bone), osteonal arrangement (e.g. reticular to plexiform), degree of vascularity (decreases as growth slows) and/or collagen fibre organisation (increases as growth slows). Juveniles have been described as bearing relatively homogenous bone, and even in those with some zonation, lack of change between zones is considered an immature characteristic (Martin et al., 2024).

3.3.3 | Changes in zone thickness/spacing of CGMs

The spacing between CGMs (LAGs and annuli), and thus the width of the zones between them (which are numbered based on the outer CGM bordering them, i.e. zone 2 is between CGM 1 and CGM 2), forms the basis for tracking growth over time and constructing histological growth curves. The periodicity of these growth lines has led authors to interpret them as occurring annually corresponding to seasonal periods of higher physiological stress (Horner et al., 2001; Varricchio, 1993). In extant animals, this has been tested using fluorescent labelling to track changes in bone (*Crocodylus niloticus*, Hutton, 1986; *Varanus niloticus*, de Buffrénil & Castanet, 2000; *Microcebus murinus*, Castanet et al., 2004). In fossils, however, fluorescent labelling is not possible, so isotope geochemistry may be used to track changes in isotope composition throughout the cortex (Padian & Lamm, 2013). One study on sauropods from the Shishugou Formation of China found regular increases in proportions of $\delta^{18}O$ (associated with drier climate) corresponding to growth marks suggesting seasonality and supporting annual periodicity (Tütken et al., 2004). Previous authors have proposed that like in extant crocodilians and squamates, an abrupt change in the spacing of CGMs corresponds to the onset of sexual maturity wherein energy allocation shifts from growth to reproduction (Andrews, 1982; Gianechini et al., 2018; Martin et al., 2024; Shen, Zhao, et al., 2017; Shine & Charnov, 1992). This is contrary to birds that often reach sexual maturity following somatic maturity, sometimes even years later (Ricklefs, 1968). See the Discussion section for caveats regarding these interpretations. Regardless of whether it represents sexual maturity, an abrupt decrease in growth mark spacing and subsequent plateau where growth marks (typically LAGs) begin to appear closely packed together in the periosteal cortex is interpreted as a subadult characteristic.

3.3.4 | Deposition of an EFS

When LAGs have become very tightly spaced and the outermost layers are devoid of primary osteons and vascularity (forming an EFS), the individual is interpreted as a skeletally mature adult that has ceased growth (de Buffrénil & Quilhac, 2021).

3.4 | Graphing growth

Preliminary sections revealed that MTIIIs did not show as complete a growth series as MTIIs and MTIVs due to extensive remodelling mediolaterally and posteriorly. These regions are associated with contacts between MTII and MTIV, which likely contribute to their relatively limited growth plane. Therefore, primary assessments of growth rates were done using MTII and MTIV samples.

Images of thin sections were loaded into ImageJ and scaled to millimeters using the line-scaling tool. For each identified CGM, the circumference was outlined using the polygon selection tool and the inner area was measured using the measure function. In cases where the medullary cavity had expanded over parts of a growth mark, the preserved parts were connected by tracing the border of the medullary cavity to avoid speculation of the missing shape. Furthermore, in cases where remodelling has obstructed our ability to follow CGMs, they were estimated by drawing a path following the outer edge of the cortex from the same distance away as where the growth mark was last visible. Multiple/split LAGs were traced throughout the cortex to determine if they truly were split, in which case only the outer line was measured as per Cullen, Brown, et al. (2021). Given the expansion of the medullary cavity as the animals grew, we employed retrocalculation methods to determine whether there were any missing growth marks once present deep within the cortex. These methods vary throughout the literature and are case by case (Cullen, Brown, et al., 2021; Horner et al., 2001). Here, we employ an image-stacking technique wherein histological images with traced CGMs corresponding to the same region of bone were set to the same scale and overlain one over the other so that the growth marks were matched as closely as possible. If the medullary cavity

of a particular specimen was large enough that it had expanded over the innermost growth marks of other, typically smaller specimens with smaller medullary cavities, it was assumed that it had lost those growth marks. This methodology was used instead of a model-based approach given that estimating the total age of each specimen was not the focus of the study as much as simply comparing growth trajectories. Thus, we only needed enough information about missing CGMs to 'line up' the specimens so that the growth zones across specimens all correspond to the same period of growth. Any CGMs that might be completely absent across all of our specimens (i.e. in the case, none of the juveniles were young enough to preserve them) were irrelevant. Areas for all growth marks within a specimen were imported into PAST v4.08 (Hammer & Harper, 2001) and graphed in a biplot against the number in sequence from the medullary cavity. All specimens of the same metatarsal at comparable cut locations were plotted against each other to examine trends.

4 | RESULTS

4.1 | Troodontid metatarsal osteohistology

4.1.1 | Metatarsal II

The distal shaft sections of MTII are typically oval in cross-section and the medullary cavity is similar in proportions, with a long axis that aligns with that of the overall cross-section (Figure 2). However, TMP1992.036.0720, which is interpreted as pathologic, is an exception as the lateral margin is slightly concave as opposed to convex and the anterior–medial region balloons outward forming an unusual silhouette that is further exaggerated moving proximally (Figure 2b). In all specimens, the border of the medullary cavity is lined with an IFS of avascular lamellar bone (ALB), but its thickness varies. The cortex is composed predominantly of woven-parallel complexes with a mixed arrangement of osteons, typically in a reticular pattern

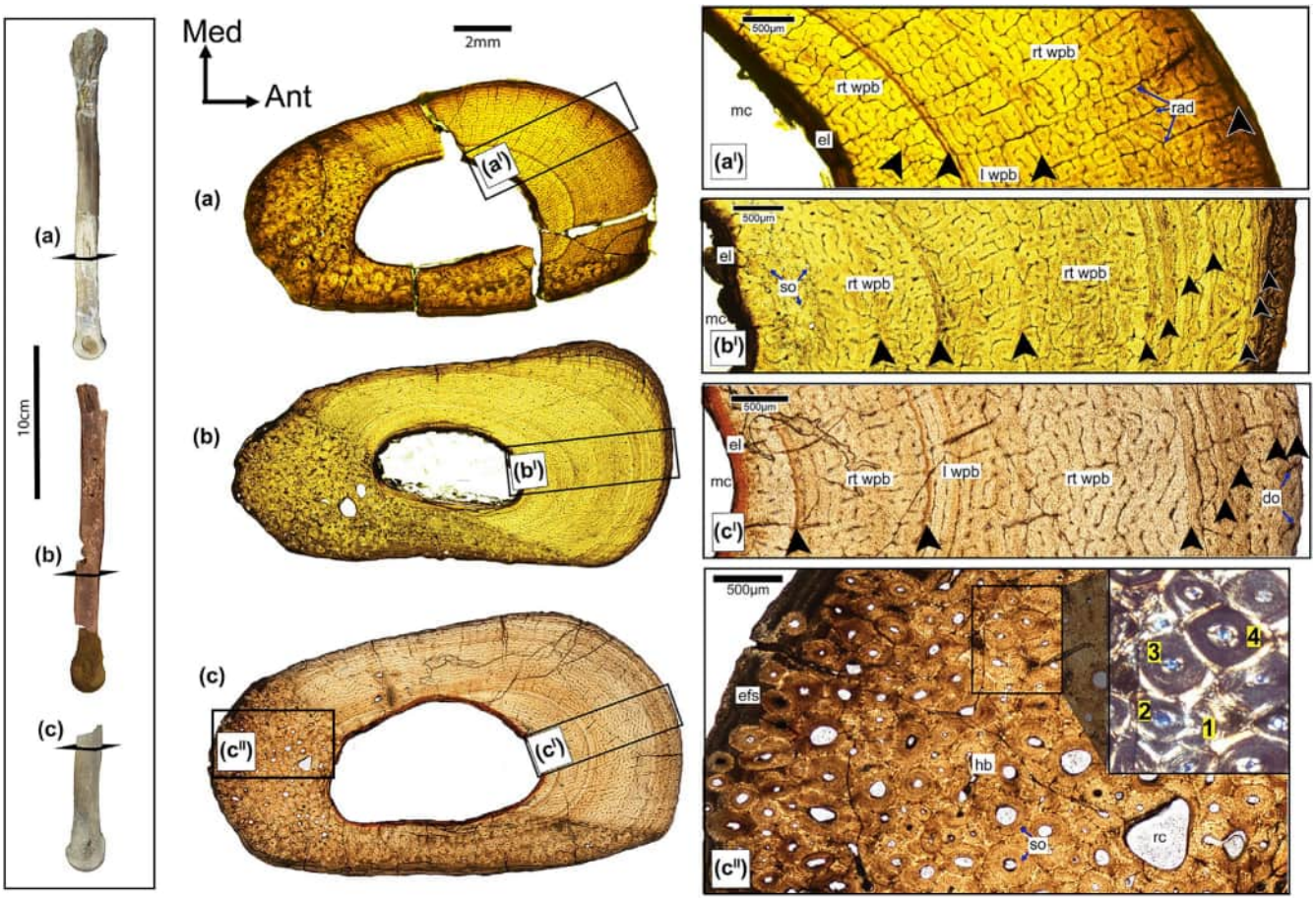

FIGURE 2 Osteohistological thin sections of three troodontid metatarsal IIs (MTIIs) from the Dinosaur Park Formation. Specimen photographs are in lateral view. Arrowheads indicate cyclical growth marks (lines of arrested growth [LAGs] and annuli). do, developing osteon; efs, external fundamental system; el, endosteal lamellar bone; hb, Haversian bone; l wpb, lamellar woven-parallel bone; mc, medullary cavity; rad, radial vasculature; rc, resorption cavity; rt. wpb, reticular woven-parallel bone; so, secondary osteon. (a) Thin section of TMP1994.012.0884. (a^{I}) Detail of the primary bone cortex of TMP1994.012.0884. (b) Thin section of TMP1992.036.0720. (b^{I}) Detail of the primary bone cortex of TMP1992.036.0720. (c) Thin section of TMP1999.055.0118. (c^{I}) Detail of the primary bone cortex of TMP1999.055.0118. (c^{II}) Detail of the secondary remodelled bone cortex of TMP1999.055.0118. Inset image shows cross-polarised light detail of four generations of stacked secondary osteons.

with some laminarity associated with LAGs and closer to the periosteum. CGMs in the form of LAGs and circumferential bands of parallel-fibered bone (PFB) interpreted as annuli were present in all three specimens. The largest MTII (TMP1999.055.0118) has eight visible CGMs, whereas the smallest has three, possibly four. The zones marked by these growth marks varied in thickness but featured a prominent increase in thickness between zone 2 and 3 for TMP1992.036.0720 and TMP1999.055.0118, and between zone 3 and 4 for TMP1994.012.0884. These were only interrupted in the posterior and lateral aspects of the sections where the tissue was more osteocyte lacunae dense and dominated by secondary osteons forming a Haversian bone system. The largest MTII (TMP1999.055.0118) had at least four generations of secondary osteons in the Haversian tissue region, whereas the smallest (TMP1994.012.0884) appears to have two generations (Figure 2c^{II}).

4.1.2 | Metatarsal III

The microanatomy of MTIII varied between individuals but sections were taken from different regions along the shaft, so direct comparisons are less reliable. However, the shaft of MTIII is strongly triangular in all cross sections observed with woven-parallel complexes of mixed osteonal arrangements along the anterior aspect, and disorganised bone of longitudinal orientation but dense secondary osteons throughout the posterior apex and the lateral and medial aspects (Figure 3). In TMP1998.068.0090, there is one large medullary cavity with a much smaller cavity immediately posterior to it surrounded by porous bone containing secondary osteons (Figure 3a). The primary bone of this individual was reticular within the inner third and more laminar in the outer two-thirds, especially along the anterior-most aspect. In the other two MTIIIs (TMP1997.0133.0008 and TMP2005.049.0015), the medullary cavity is more chambered, with each cavity bordered by a few layers of endosteal ALB (Figure 3b,c). This region also has many additional cavities formed by resorption given the numerous secondary osteons. The primary woven-parallel complexes in these two individuals showed a different osteonal arrangement, containing a mix of longitudinal osteons towards the lateral apex and reticular to sub-plexiform towards the medial apex. Closer to the periosteum in the outer quarter however, the bone exhibits greater zonation, with alternating layers of slower-growing PFB and circumferential rows of primary osteons (Figure 3b^{I},c^{I}). Unlike MTII, CGMs were less common and less discernible in MTIII. TMP1998.068.0090

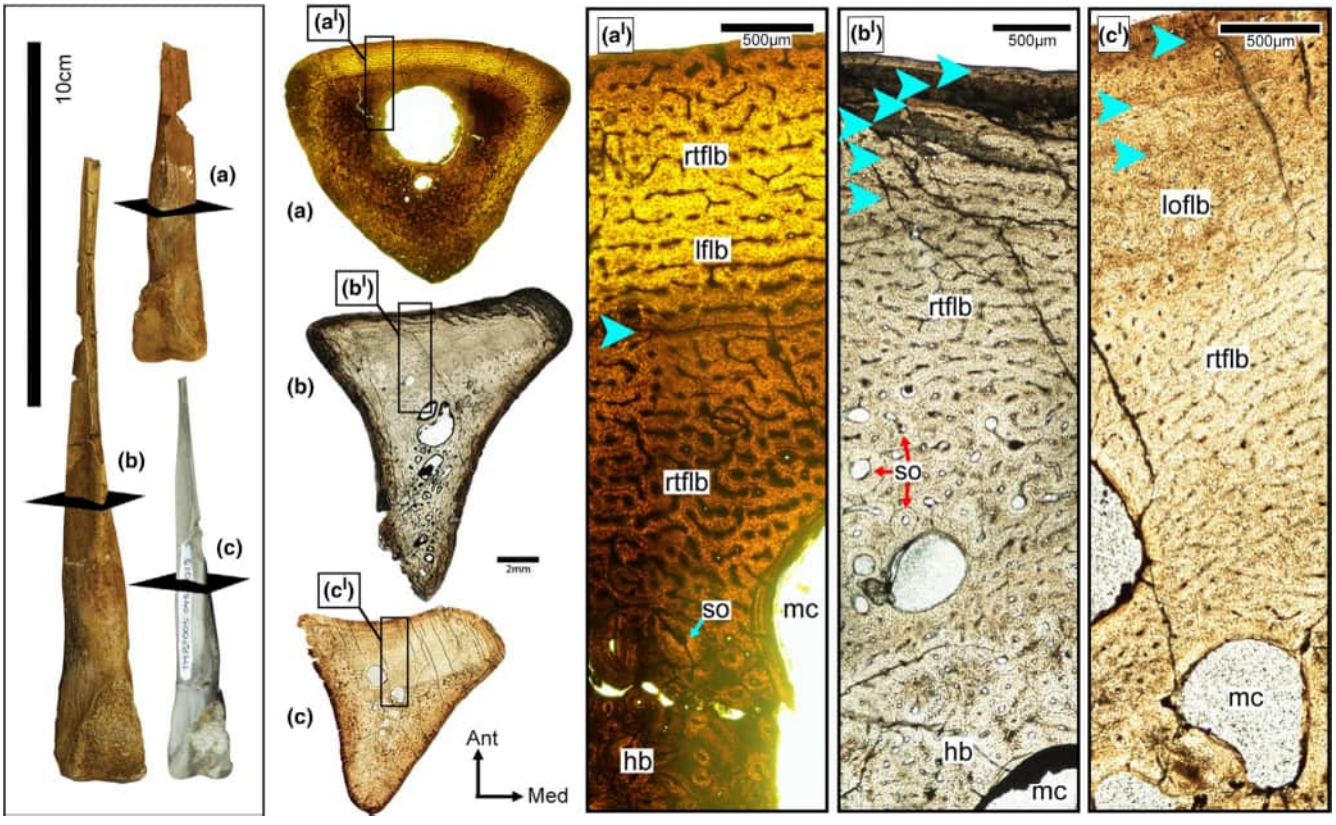

FIGURE 3 Osteohistological thin sections of three troodontid metatarsal IIIs (MTIIIs) from the Dinosaur Park Formation. Specimen photographs are in posterior view. Arrowheads indicate cyclical growth marks (lines of arrested growth [LAGs] and annuli). hb, Haversian bone; l wpb, lamellar woven-parallel bone; lo wpb, longitudinal woven-parallel bone; mc, medullary cavity; rt. wpb, reticular woven-parallel bone; so, secondary osteon. (a) Thin section of TMP1998.068.0090. (a^{I}) Detail of the primary bone cortex of TMP1998.068.0009. (b) Thin section of TMP1997.133.0008. (b^{I}) Detail of the primary bone cortex of TMP1997.133.0008. (c) Thin section of TMP2005.049.0015. (c^{I}) Detail of the primary bone cortex of TMP2005.049.0015.

had one CGM, TMP2005.049.0015 had at least two CGMs and TMP1997.0133.0008 had at least four CGMs.

4.1.3 | Metatarsal IV

MTIV was the most extensively sampled element both in the number of individuals and in the number of regions along the bone (Figure 4). As a result, a variety of bone microstructural characteristics were observed across the samples. At the distal-most end of the shaft, MTIV is roughly teardrop to square in cross section, with a rounded medullary cavity occupying ~12% of the section (Figure 4). Moving proximally, the articular surface with MTIII reduces in size and tapers, resulting in more triangular cross sections (Figure 5). The medullary cavity also occupies a greater proportion of the cross-sectional area (~23%) more proximally. All MTIV sections consist predominantly of woven-parallel complexes exhibiting a mixture of different primary osteon arrangements. The most common was a reticular matrix, especially within the inner two-thirds of the cortex (Figures 4a^{I},b^{I} and 5a^{I},b^{I},c^{I}). Radial vasculature was present predominantly towards the anterior aspect of MTIV and more prevalent in the outer cortex. The exception is TMP2005.049.0086, where long radial channels were conspicuously absent (Figures 4b and 5b). Instead, the outer half of the cortex of this specimen was dominated by longitudinal osteons (Figures 4b^{I} and 5b^{I}). Laminar or sub-plexiform osteonal arrangements do occur, but they are typically concentrated in the anterior–medial regions of the proximal shaft sections (Figure 1a^{I}) and/or associated with CGMs. CGMs including LAGs and annuli were observed in every section and varied in number from ~7 to 10. However, they were interrupted by regions dense in osteocyte lacunae featuring secondary osteons (Figure 1a–c), identified by their discrete borders (resorption/cementing lines),

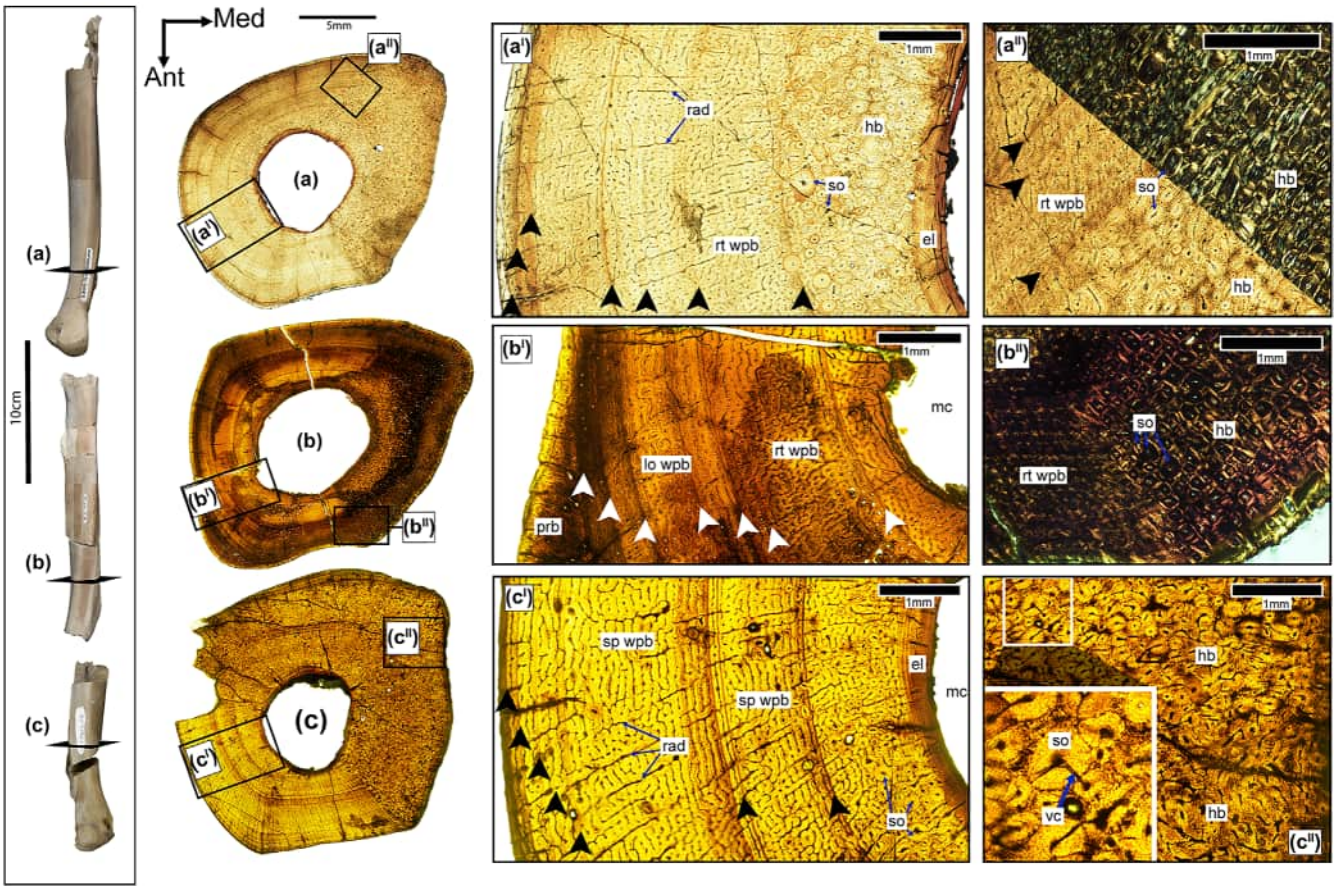

FIGURE 4 Osteohistological thin sections from the distal shaft region of three troodontid metatarsal IVs (MTIVs) from the Dinosaur Park Formation. Specimen photographs are in anterior view. Arrowheads indicate cyclical growth marks (lines of arrested growth [LAGs] and annuli). el, endosteal lamellar bone; hb, Haversian bone; lo wpb, longitudinal woven-parallel bone; mc, medullary cavity; prb, periosteal reactive bone; rad, radial vasculature; rt wpb, reticular woven-parallel bone; so, secondary osteon; sp. wpb, sub-plexiform woven-parallel bone; vc, Volkman's canal. (a) Thin section of TMP2003.012.0065. (a^{I}) Detail of the primary bone cortex of TMP2003.012.0065. (a^{II}) Detail of the transition between the primary and the remodelled secondary bone-dominant region of the cortex of TMP2003.012.0065. Bottom left is polarised light and top right is cross polarised. (b) Thin section of TMP2005.049.0086. (b^{I}) Detail of the primary bone cortex of TMP2005.049.0086. (b^{II}) Detail of the transition between the primary and the remodelled secondary bone-dominant region of the cortex of TMP2005.049.0086 in crossed-polarised light. (c) Thin section of TMP1999.055.0118. (c^{I}) Detail of the primary bone cortex of TMP1999.055.0118. (c^{II}) Detail of the secondary bone-dominant region of the cortex of TMP1999.055.0118. Inset image shows a secondary osteon in closer detail.

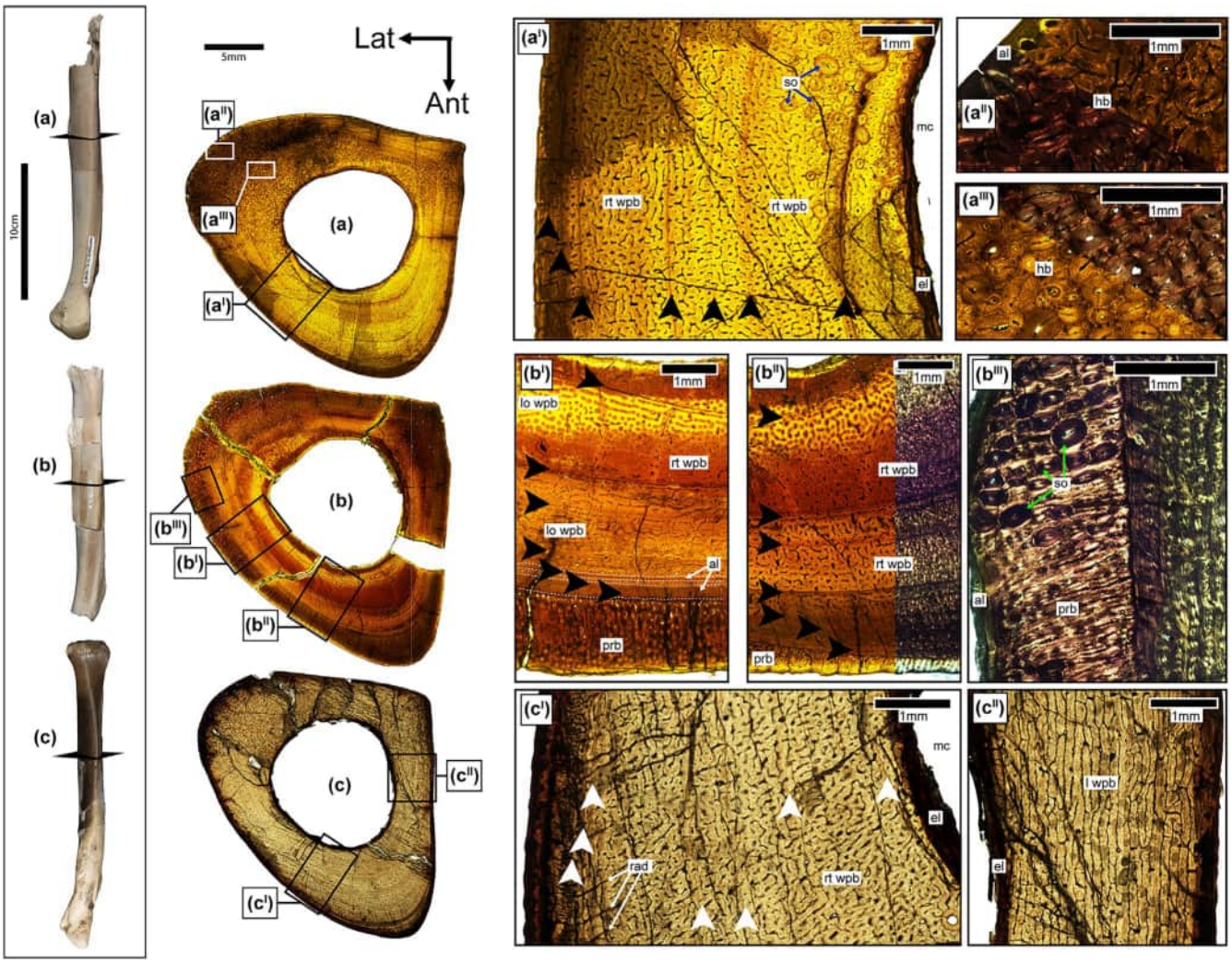

FIGURE 5 Osteohistological thin sections from the midshaft region of three troodontid metatarsal IVs (MTIVs) from the Dinosaur Park Formation. Specimen photographs are in anterior view. Arrowheads indicate cyclical growth marks (lines of arrested growth [LAGs] and annuli). al, subperiosteal avascular lamellar bone; el, endosteal lamellar bone; hb, Haversian bone; l wpb, laminar woven-parallel bone; lo wpb, longitudinal woven-parallel bone; mc, medullary cavity; prb, periosteal reactive bone; rad, radial vasculature; rt. wpb, reticular woven-parallel bone; so, secondary osteon. (a) Thin section of TMP2003.012.0065. (a^{I}) Detail of primary bone cortex of TMP2003.012.0065. (a^{II}, a^{III}) Detail of the secondarily remodelled region of the cortex of TMP2003.012.0065 in both normal and cross-polarised light. (b) Thin section of TMP2005.049.0086. (b^{I}, b^{II}) Detail of the primary bone cortex of TMP2005.049.0086. Dotted white lines delineate boundaries of avascular lamellar bone regions bordered by LAGs. (b^{III}) Detail of the periosteal reactive bone of TMP2005.049.0086 in crossed-polarised light. (c) Thin section of TMP1967.020.0026. (c^{I}–c^{II}) Detail of the primary bone cortex of TMP1967.020.0026. (c^{II}) Detail of the region of the primary bone cortex of TMP1967.020.0026 that is dominated by laminar woven-parallel bone.

size, crosscutting and anastomoses between vasculature of adjacent osteons (Figure 4c^{II}). They ranged from being oriented longitudinally (albeit disorganised rather than in circumferential rows) to disorganised, with their long axes oriented in various directions. In the distal sections, this Haversian tissue was always found along the medial surface where MTIV articulates with MTIII (Figures 1c and 4), and in some specimens also along the lateral apex (TMP1967.020.0026, TMP1992.036.0720 and TMP1999.055.0118) (Figures S11, S9 and S4, respectively). Moving proximally, the medial remodelled tissue became less widespread as the articular surface with MTIII tapered but became more prominent along the lateral apex, which itself has shifted posteriorly (Figure 1a,b).

4.2 | Pathological descriptions

Of the nine individuals sampled, three of them presented with pathologies. Two were isolated MTIVs, but one, TMP1992.036.0720, consisted of an associated MTII and MTIV, both showing evidence of pathology.

4.2.1 | TMP1967.020.0026

This complete right MTIV exhibits an abnormal expansion of periosteal reactive bone on the anterior surface of the diaphysis

forming a swell about 55 mm long proximodistally and beginning ~42.7 mm from the distal-most end of the metatarsal (Figure 6a). The swell is not abrupt and instead rises gradually from the normal extent of the cortex, so it is difficult to measure exactly where it begins and ends. The surface of the swell is smooth but with a slight undulating 'wavy' texture. Histology revealed that the swell extended ~3 mm out from the normal margin of the cortex at its thickest point.

Two histological cross sections were taken from this bone: one from where the swell was at its widest (67IV-1) (Figure 6) and another more proximally close to the midshaft where no external pathological features were observed (67IV-2) (Figure 5c). This is reflected histologically as well, for within section 67IV-2 no overt pathologic structures can be seen. Within section 67IV-1 however, extensive pathological bone is present. It extends along the entire anterior surface, terminating medially where the flat articular surface with

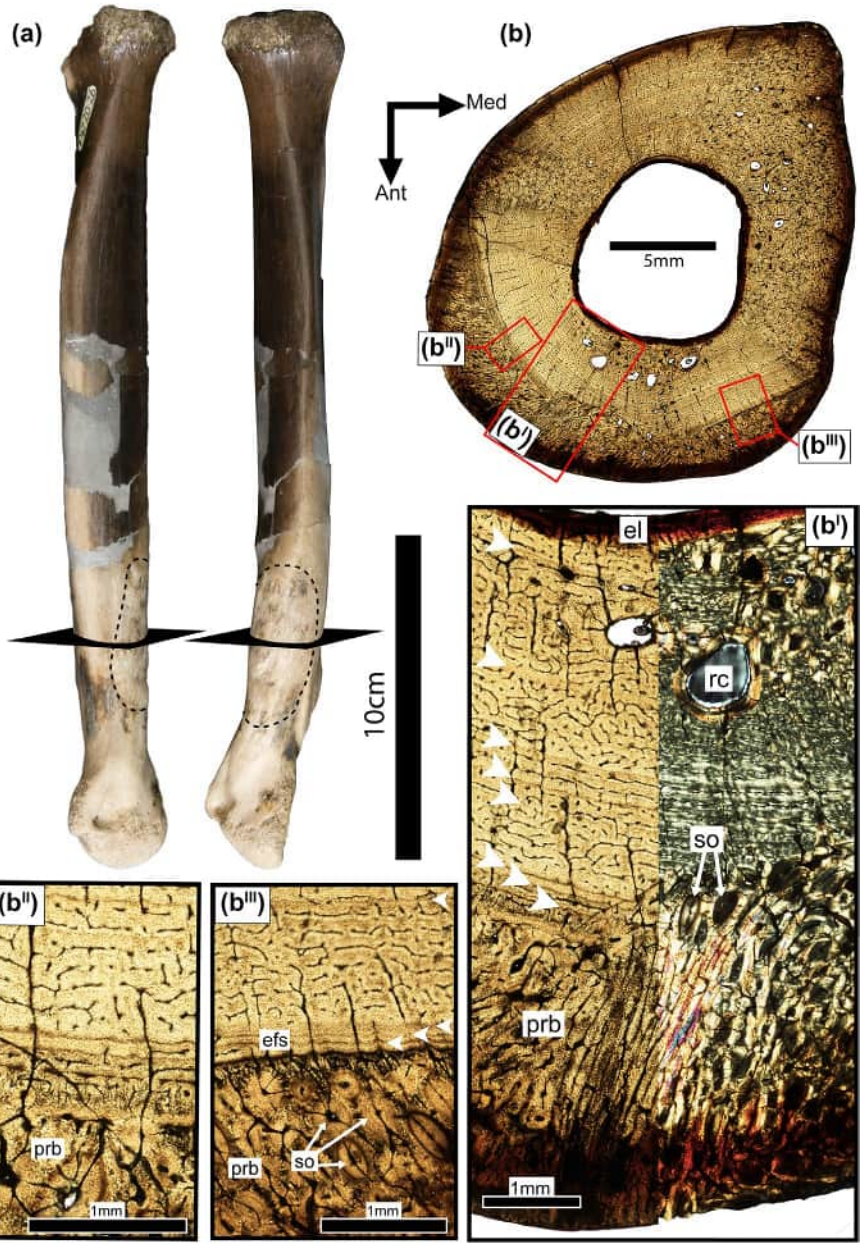

FIGURE 6 Gross morphology and osteohistology of TMP1967.020.0026 pathologic right metatarsal IV. (a) Photographs of the specimen in lateral and anterior view. Black dotted line indicates the approximate border of the pathologic periosteal reaction. (b) Thin section of the distal shaft pathologic region of TMP1967.020.0026. White arrowheads indicate cyclical growth markers (lines of arrested growth [LAGs] and annuli). efs, external fundamental system; el, endosteal lamellar bone; prb, periosteal reactive bone; rc, resorption cavity; so, secondary osteon. (b^{I}) Detail of the normal primary bone cortex and pathologic region of periosteal reactive bone that disrupts the normal contours of the outermost LAGs. (b^{II}) Detail of the boundary between the periosteal reactive bone and regular primary bone cortex where the normal deposition of an EFS is interrupted by a layer of hypervascularised non-radial tissue. (b^{III}) Detail of the region of transition between the normal primary bone of the cortex featuring a normal regional external fundamental system and the periosteal reactive bone.

MTIII begins and laterally at the anterolateral apex (Figure 6b). The swell of periosteal reactive bone is characterised by dense, highly vascularised and osteocyte-rich woven-fibered trabeculae scaffolding infilled with parallel-fibered and lamellar bone. This bone is far more disorganised than the normal cortical primary bone, but some directionality is present in the vasculature, which is predominantly radially oriented (Figure 6b^{I}). Additionally, there are many secondary osteons throughout the swell, and while some are oriented longitudinally, many are oriented randomly (Figure 6b^{III}). Anastomoses between the Haversian canals of the secondary osteons are also prolific. While the reactive bone is predominantly located external to the normal cortex, there is a region anteriorly where some of it 'invades' and truncates the normal primary bone (Figure 6b^{I}). In the region along the endosteal margin, there is also a large cluster of secondary osteons and a few larger resorptive cavities lined with lamellar bone. Internal to the pathology, the cortex is composed of normal woven-parallel bone and localised Haversian bone consistent with what was typically observed for MTIV. An EFS is present interior to the periosteal reactive bone but interrupted in some regions by invading pathological bone and secondary remodelling (Figure 6b^{I}) and in other regions by a lens of hypervascularised non-radial tissue (Figure 6b^{II}).

4.2.2 | TMP2005.049.0086

This right MTIV consists of most of the length of the shaft and is missing only the distal and proximal ends. Along the posterolateral ridge, ~170 mm from the estimated distal end, there is an outgrowth ~19 mm long and ~8 mm wide that is rough, porous and irregular in texture. Distal to the outgrowth along the posterolateral ridge, the bone also appears to have a slightly wavy yet smooth texture.

Three histological cross sections were taken from this bone: the distal region (05IV-1) (Figure 4b), the shaft just distal to the pathology (05IV-2) (Figure 5b) and the most prominent part of the pathological outgrowth (05IV-3) (Figure 7). Section 05IV-1 is largely normal and consistent with what was observed in the other MTIVs: a cortex of woven-parallel reticular and longitudinal complexes and Haversian bone along the medial surface (Figure 4b). However, a small amount of periosteal reactive bone is present on the anterior apex (Figure 4b^{I}). It appears entirely remodelled by well-organised longitudinal secondary osteons. Section 0IV-2 also had a cortex composed of a woven-fibered complex but instead of Haversian bone being concentrated along the medial surface, here it is concentrated along the posterolateral apex, which corresponds to the posterolateral ridge in gross anatomical view (Figure 5b). This section also showed periosteal reactive bone but along the lateral edge. The reactive bone is predominantly composed of radially and longitudinally oriented primary osteons within a scaffolding of woven-fibered trabeculae (Figure 5b^{I}). There are some secondary osteons, but they are mostly concentrated close to the anterolateral apex. Along the external-most margin of the reactive bone, there is a thin band of parallel-fibered bone and at least a couple of LAGs are visible in some spots (Figure 5b^{III}). Section 05IV-3 was taken from the focal point of the pathological growth (Figure 7). For the most part, it is very similar to 05IV-2, but the periosteal reactive bone along the lateral margin has more disorganised vasculature (less radial) and more secondary osteons throughout. The pathological outgrowth can be seen on the posterolateral apex and extends ~3.8 mm from the regular margin of the cortex (Figure 7b^{I}). It is composed of woven-fibered trabeculae generally oriented laterally and is partially infilled with lamellar bone, but it is far more porous than the rest of the periosteal reactive bone reported for this specimen, with large vacuities throughout.

4.2.3 | TMP1992.036.0720

This is composed of a right MTII and a right MTIV. Both are missing the proximal ends but are otherwise complete. MTIV is more visibly pathologic through gross anatomical observation. The diaphysis exhibits pathological expansions throughout its length creating a 'swollen' appearance. These swells are smooth in texture and do not have abrupt margins (Figure 8). One is localised primarily towards the lateral side distally and then wraps around to the anterior surface moving proximally. At about the midshaft, there is also an additional swell along the articular surface for MTIII (Figure 9c). The most dramatic pathological feature on this bone is a highly deformed distal end. A significant amount of the bone is absent, but the surfaces in these 'reduced' regions appear to be smooth cortical bone or reactive bone as opposed to worn, porous jagged edges associated with taphonomic damage (Figure 8b–e). Several key features as a result are severely altered. The distal articular surface is blunted and oriented perpendicular to the diaphysis, as opposed to the typical convex, laterodistally oriented condition (Figure 8b,d). Both articular condyles are missing, resulting in an articular surface that is oval rather than heart shaped (Figure 8f). The articular surface is pierced by several small resorptive cavities (Figure 8f). On the medial side, the ligament pit has been posteriorly and distally displaced and is much deeper, resulting in the articular surface forming an overhang over it (Figure 8c). Similarly, on the lateral surface, the ligament pit is abnormal in shape, appearing more excavated rather than a shallow sloping basin and also has been posteriorly displaced (Figure 8e). Throughout the distal end, there are also numerous pits more disorganised in appearance than typical nutrient foramina.

Three histological sections were taken from this MTIV: 33.61 mm from the distal end (92IV-1) (Figure 9a), 59.2 mm from the distal end (92IV-2) (Figure 9b) and a midshaft section 124.3 mm from the distal end (Figure 9c). 92IV-1 is the distal-most MTIV histological section assessed in this study and thus differs a bit from the other, more proximal sections. Highly vascular and disorganised compact coarse cancellous bone, which is rare along the diaphysis, makes up the inner third of the cortex here, except along the medial aspect where it extends all the way to the periosteum but has been partially overlain by secondary osteons (Figure 9a^{II}). Additionally, unlike in the other MTIV sections, the IFS of lamellar bone in this specimen is strongly asymmetrical, being

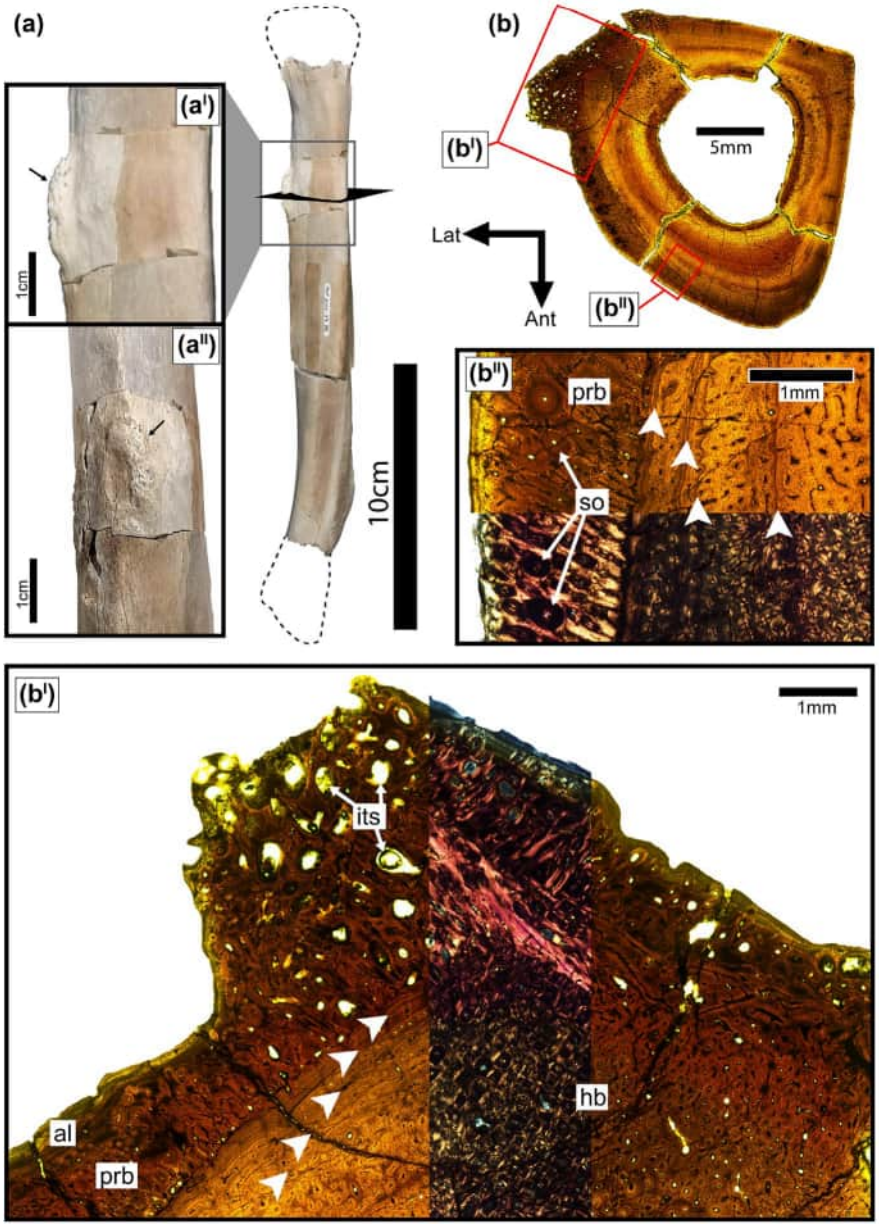

FIGURE 7 Gross morphology and osteohistology of TMP2005.049.0086 pathologic right metatarsal IV. (a) Photograph of the specimen in anterior view with black dotted line indicating the missing portions of the element. (a^{I}) Anterior detail of the pathological outgrowth indicated by arrow. (a^{II}) Lateral detail of the pathological outgrowth indicated by arrow. (b) Thin section of the pathological region of TMP2005.049.0086. White arrowheads indicate cyclical growth markers (lines of arrested growth [LAGs] and annuli). al, avascular lamellar bone; hb, Haversian bone; its, intertrabecular space; prb, periosteal reactive bone. (b^{I}) Detail of the focal region of the pathological outgrowth in normal light and cross-polarised light (central band). (b^{II}) Detail of the border between the normal primary cortical bone and the periosteal reactive bone.

narrow laterally (0.13 mm thick) and wide along the anterior, medial and posterior margins (1.02 mm at its thickest point) (Figure 9a^{II}). The pathology in 92IV-1 is characterised by a large outgrowth of periosteal reactive bone that extends 6.81 mm from the normal cortex at its widest point. It consists of a partially infilled network of somewhat radially oriented woven-fibered trabeculae. The extent of lamellar bone infilling of the intratrabecular spaces varies. It is least extensive towards the posterior-most part of the outgrowth, resulting in a more porous appearance (Figure 9a^{I}) and more extensive anteriorly. Secondary osteons are also present throughout the outgrowth and vary from predominantly longitudinally oriented closer to the external surface to radially oriented deeper within the outgrowth. Within the normal cortical bone, there are a couple of unusual features. Numerous radially oriented thick, dark, jagged lines terminate once they reach the pathological outgrowth (i.e. they do not extend through the pathology all the way to the outer surface of the bone; Figure 9a^{I}). Additionally, there are two split LAGs, one of which remarkably splits into four separate LAGs (Figure 9a^{III}). The phenomenon of double and multi-LAGs

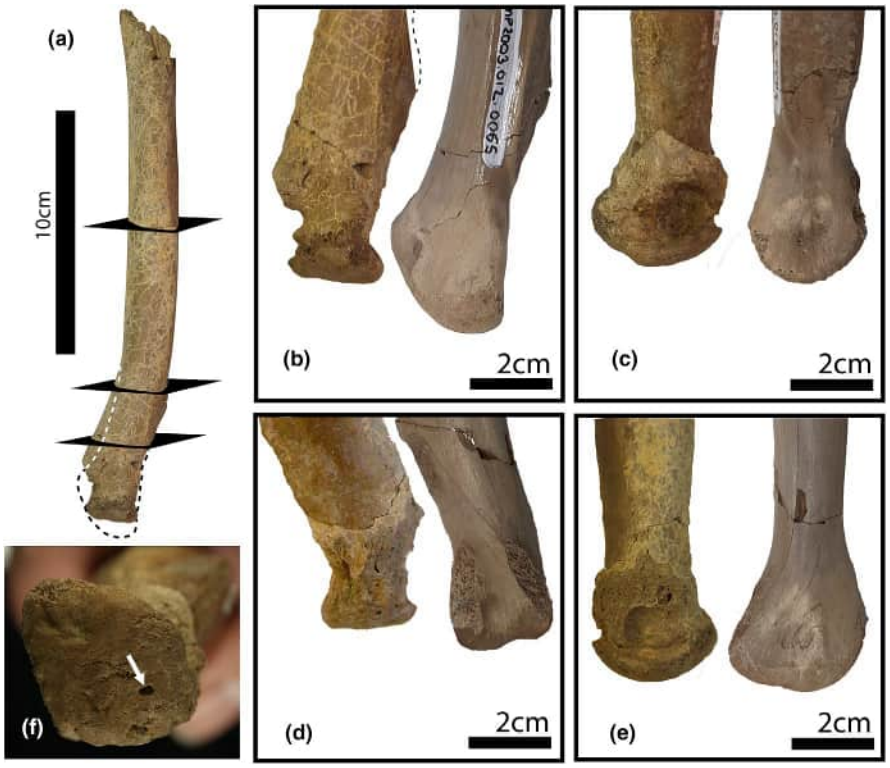

FIGURE 8 Gross morphology of the pathologic features of right metatarsal IV (MTIV) TMP1992.036.0720. (a) Photograph of the specimen in anterior view. Dotted lines show the normal contour of a healthy MTIV. Planes show where histological samples were taken. (b–e) Comparison of pathologic distal end of TMP1992.036.0720 (left) and a healthy MTIV TMP2003.012.0065 (right). (b) Anterior view. (c) Medial view. (d) Posterior view. (e) Lateral view. (f) Photograph of the distal articular surface of right MTIV TMP1992.036.0720. Arrow indicates the presence of a resorptive pit.

has been widely reported and is particularly abundant in theropods (Cullen et al., 2014, 2020; Cullen, Brown, et al., 2021; Cullen, Simon, et al., 2021; Evans et al., 2015; Jin et al., 2019; Lee & O'Connor, 2013). Split LAGs, where one splits into several closely resembling the ones seen here, have been figured previously in an immature *Gorgosaurus libratus* (FMN PR 2211) and cf. *Tyrannosaurus rex* (BMRP 2006.4.4) (Cullen et al., 2020; Cullen, Brown, et al., 2021).

Moving proximally to section 92IV-2, the pathological outgrowth becomes smaller, denser and more remodelled. More notably though is that the outgrowth features a band of PFB paired with an LAG that splits the swell into two parts (Figure 9b^{I}). Within the internal portion, the trabeculae and secondary osteons are predominantly radially oriented, whereas the external portion is dominated by longitudinally oriented secondary osteons. Like the other MTIV sections taken from this position, in the normal cortical bone, there are several radially oriented primary vascular canals (Figure 1). However, unlike the other sections, there are many radial vessels present that are secondary and formed from radially oriented secondary osteons (Figure 9b^{II}). This section has a couple split LAGs, but none as obvious or dramatic as in 92IV-1. The pathological outgrowth continues proximally as shown in section 92IV-3, which represents the mid diaphysis of this specimen (Figure 9c). The outgrowth has shifted anteriorly and is denser and more extensively remodelled, with a cluster of secondary osteons 'invading' the normal cortex along the anterior apex and disrupting the LAGs here. Unlike section 92IV-2, there are no LAGs dividing the pathology into sections, so the osteohistology of the outgrowth when moving from internal to external appears more uniform. Most of the secondary osteons in the pathological region are longitudinal, but some are still more radially oriented along the lateral margin. Unlike section 92IV-2, an additional region of periosteal reactive bone is present along the posteromedial aspect. This one is bordered along the external margin by a band of primary osteons and PFB containing up to three LAGs and is extensively remodelled, containing at least three generations of secondary osteons (Figure 9c^{II}).

MTII appeared mostly normal through gross anatomical inspection except for a slight depression along the lateral surface creating a sharper ridge along the posterolateral surface than is typical. Histologically, however, the pathological features are more obvious. Two cross-sections were taken from the midshaft region: 92II-1 (distal) (Figure 2b) and 92II-2 (proximal) (Figure S7). 92II-1 was more informative overall as it was the only one directly comparable to the other two specimens of MTII assessed based on anatomical position. This revealed an unusual silhouette (Figure 2b). Instead of a slightly convex or flat lateral edge, 92II-1 is slightly concave, with the LAGs also following the curvature and bowing towards the medullary cavity as opposed to remaining flat. The posterior edge of the bone also appears irregular, protruding out slightly instead of forming a smooth curve. Finally, the anteromedial corner balloons outward beyond the

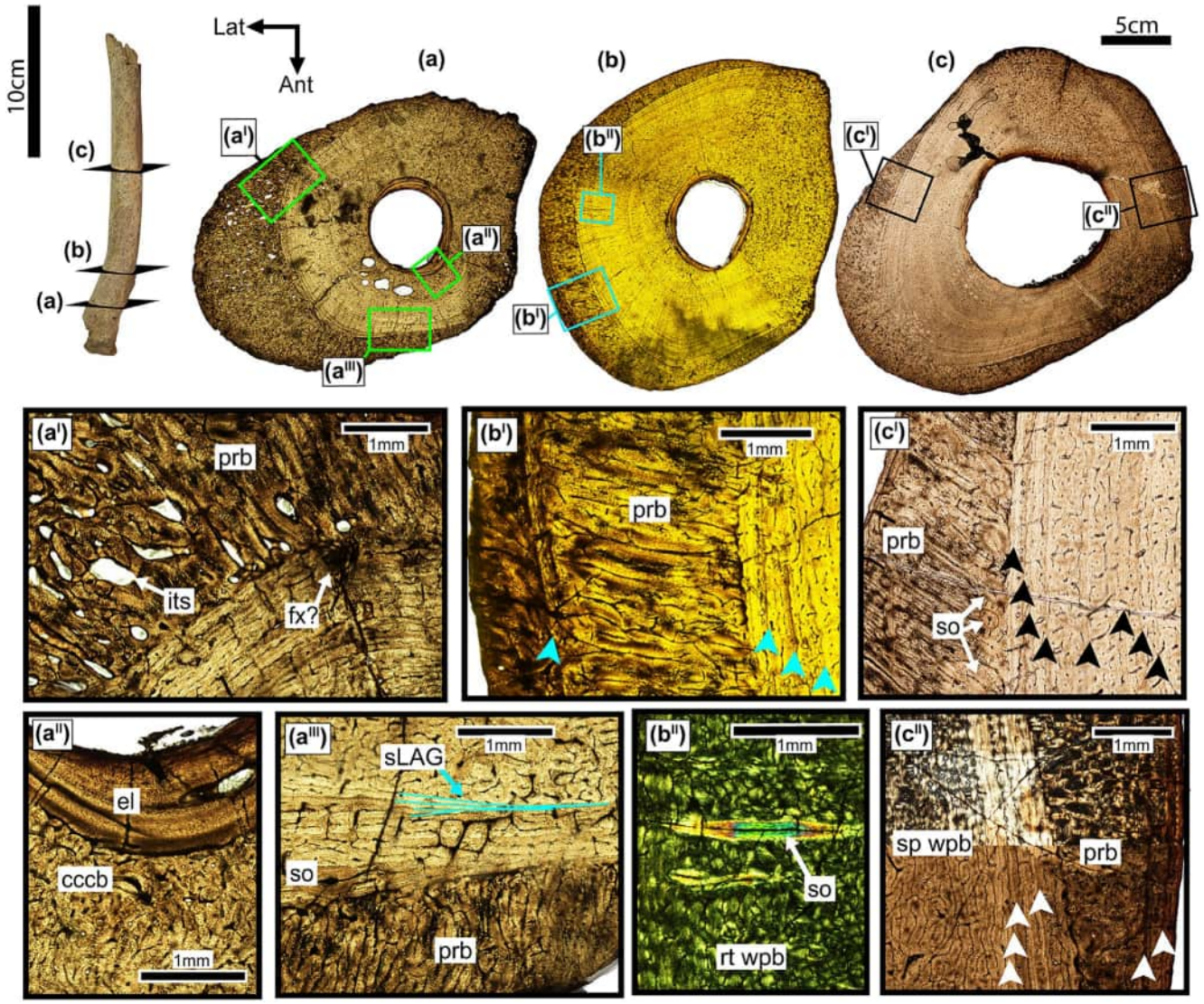

FIGURE 9 Gross morphology and osteohistology of TMP1992.036.0720 pathological right metatarsal IV. Photograph of the specimen in anterior view. (a–c) Thin sections of TMP1992.036.0720. Arrowheads indicate cyclical growth marks (lines of arrested growth [LAGs] and annuli). cccb, compact course cancellous bone; el, endosteal lamellar bone; fx?, possible fracture; its, intratrabecular space; prb, periosteal reactive bone; rt. wpb, reticular woven-parallel bone; sLAG, split LAG; so, secondary osteon; sp. wpb, sub-plexiform woven-parallel bone. (a) Histological section of the lower distal shaft. (a^{I}–a^{III}) Details of the distal-most shaft section. (b) Histological section of the upper distal shaft. (b^{I}) Detail of the upper distal shaft section in normal light. (b^{II}) Detail of the upper distal shaft section in cross-polarised light. (c) Histological section of the midshaft region. (c^{I}) Detail of the midshaft sections in normal light. (c^{II}) Detail of the midshaft section in normal light (lower) and cross-polarised light (upper).

regular margin of the cortex. Unlike the previously discussed pathological bones wherein most of the abnormal growth was periosteal, here it is the primary bone of the cortex that contributes the most to the unusual shape; however, there is a small layer of periosteal reactive bone. Within this region of excess primary cortical bone growth, three sets of split LAGs are present. In section 92II-2, this expansion is even larger (92II-2) and contains up to five sets of split LAGs (Figure S7). On the opposite side along the posterolateral corner, there is also a protrusion of bone continuous with the primary bone of the cortex that corresponds to the sharp ridge previously noted. The bone within this protrusion is disorganised and osteocyte rich and appears similar to compact coarse cancellous bone. This bone texture is also present within the interior half of the cortex posterior to the medullary cavity.

4.3 | Distribution of qualitative ontogenetic features

The sampled metatarsals varied in absolute dimensions and qualitative ontogenetic features (Table 1). Across all individuals, however, at least one CGM was present. Additionally, all specimens had developed an IFS of endosteal lamellar bone and had undergone some local secondary remodelling. The next

most frequently observed marker was a sudden decrease in zone thickness (area between CGM) and continued deposition of closely packed growth marks (predominantly LAGs). All but two individuals (TMP1994.012.0884 and TMP1998.068.0090) had this sudden decrease in zone thickness, and it typically occurred following the fourth or sixth growth mark. This sudden decrease in zone thickness was also associated with the most prominent change in bone structure (vasculature orientation/density or fibre type): an increased prevalence of slow-growing parallel-fibered bone (PFB) or lamellar bone in between CGMs and circumferential layers of osteons. However, other changes in fibre type and vasculature between zones were individually variable and inconsistent with any patterns in CGM deposition. Topographic location was more important (e.g. anterior vs. lateral aspect). For example, radial vasculature was more common anteriorly in MTII and MTIV, and laminar vasculature was more common medially and posteriorly in the upper shaft of MTIV (Figure 1). The presence of an EFS was only considered when closely packed alternating layers of LAGs and avascular bone lacking developing osteons were observed. A full EFS around the entire circumference of the cortex was rare if present at all. Both sections of MTII of TMP1992.036.0720 had the most extensive and obvious EFS, but it is worth noting that the pathologies in this specimen resulted in an unusual cross section with double and multi-LAGs regionally and periosteal reactive bone making an EFS difficult to follow. Most specimens with an EFS had it localised to certain regions of the periosteum, corresponding to the regions that were remodelled (Figure 1). While most specimens were isolated, two individuals had associated elements permitting direct comparison. TMP1999.055.0118 consisted of an MTII and an MTIV, and both had ~8 CGMs. The pathological individual TMP1992.036.0720 also consisted of an MTII and an MTIV. However, given the pathology and the resulting unusual shape and occurrence of split LAGs and multi-LAGS, only the LAGs that could be circumferentially traced throughout the cortex were considered as representing CGMs. This resulted in ~10 for both MTII and MTIV.

4.4 | Variation of growth rates within individuals

In the sample, only two specimens had more than one element available for histology: TMP1992.036.0720 and TMP1999.055.0118, each consisting of an MTII and an MTIV. The growth trajectories between elements within an individual were remarkably similar, with proportionally similar zone spacing throughout (Figure 10). Only one of three sections (92IV-3) for TMP1992.036.0720 preserved an extra CGM (10), while the other MTIV and the MTII sections both had nine. Meanwhile, both the MTII and MTIV sections of TMP1999.055.0118 preserved seven CGMs (not including any retrocalculated missing CGMs). This allows for greater confidence when comparing between different metatarsals in our sample.

4.5 | Growth trajectories

Comparing all the metatarsals together, two growth trajectories are apparent. Considering MTII independently, growth appears to follow a slightly logistic growth, beginning growth slowly from CGM 1 through to CGM 3 and followed by an abrupt increase in growth from CGM 3 to CGM 4 and subsequent plateau (Figure 11). Two of the MTII specimens conform closely to each other: TMP1994.012.0884 and TMP1999.055.0118, the former ceasing at CGM 4 before its growth was expected to have slowed. However, the pathologic TMP1992.036.0720 appears to have had a reduced growth period between CGM 3 and CGM 4, failing to reach a comparable size to the other two when its growth begins to plateau (Figure 11). Despite this, it still follows a similar pattern of growth accelerations and decelerations. The associated MTIVs from TMP1992.036.0720 and TMP1999.055.0118 follow a similar pattern as seen in their corresponding MTIIs, wherein the largest region of growth occurs between CGM 3 and 4, followed by a subsequent decrease in growth area and plateau (Figure 12b). Other metatarsals, TMP1967.020.0026, TMP2003.012.0065 and TMP2005.049.0086 exhibit steadier growth with more even spacing between CGMs up until CGM 6 where growth begins to plateau (Figure 12). This pattern is also consistent between sectioned regions of MTIV, with the distal and proximal sections both showing the same trend. Of the three specimens, two were pathologic: TMP1967.020.0026 and TMP2005.049.0086. However, given that all three specimens, including the non-pathological one, follow a similar growth trajectory, it does not seem that the pathologies are a factor for this discrepancy between the two different growth trajectories observed in the sample.

5 | DISCUSSION

5.1 | Troodontid metatarsal osteohistology

5.1.1 | Reticular woven-parallel complexes and the speed of maturation

Consistent with what has been previously reported for Troodontidae, the bone architecture of the metatarsals consisted of an endosteal lamellar component forming an ICL, and a periosteal-derived cortex of predominantly woven-parallel bone interspersed with CGMs (LAGs and/or annuli) and greater abundance of parallel-fibered or lamellar bone towards the periosteum (Martin et al., 2024). Of the variety of woven-parallel complex osteonal arrangements reported, reticular woven-parallel complexes were by far the most common. These complexes dominated the majority of the cortex in the specimens comprising its entirety or in cases where multiple types of WPCs were observed, typically localised to the interior. The predominance of reticular bone, particularly within the deeper cortex, is consistent not only with what has been previously reported for troodontids (Martin et al., 2024)

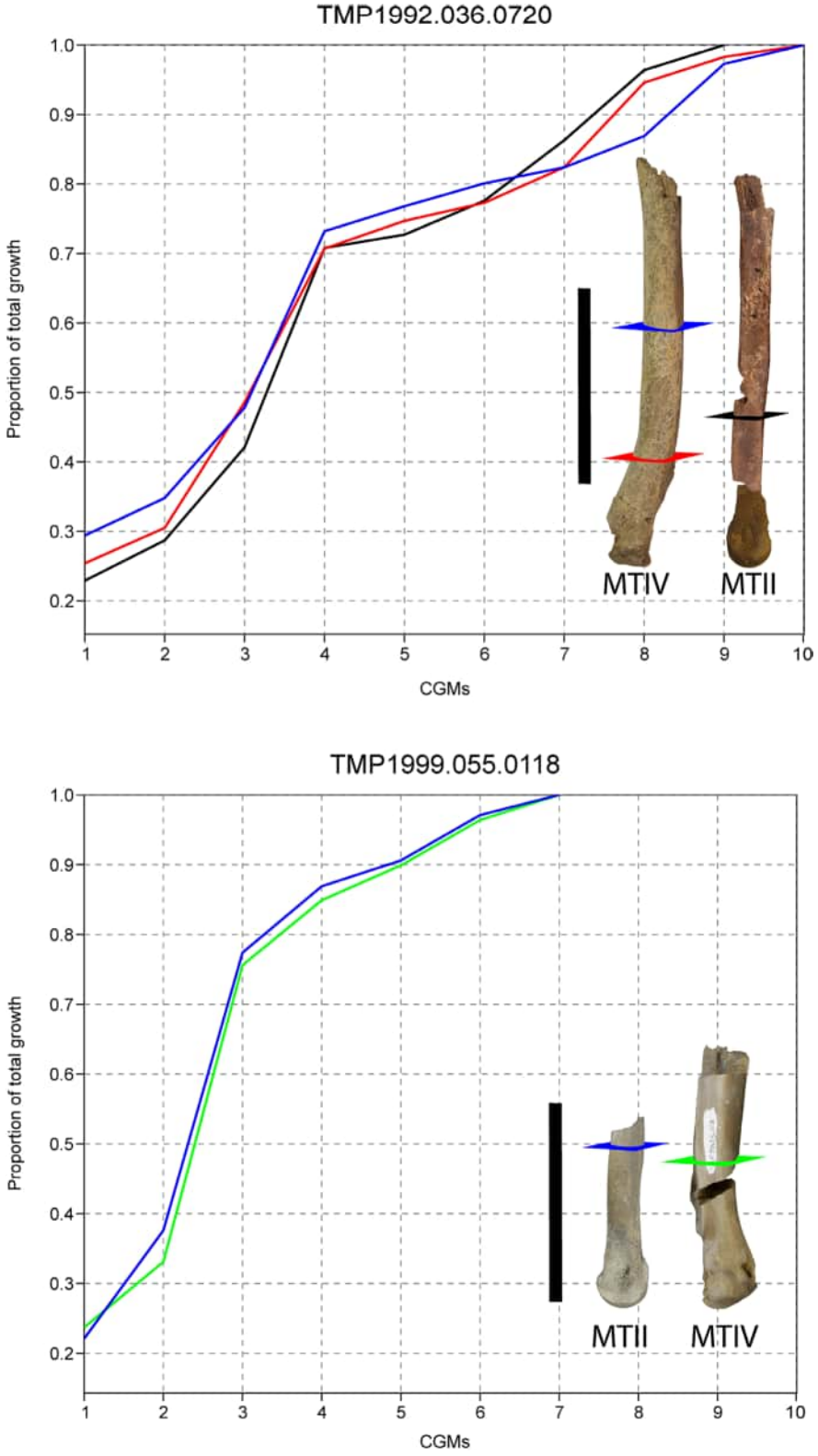

FIGURE 10 Cumulative growth graphs for the two individuals preserving two associated metatarsals (TMP1992.036.0720 and TMP1999.055.0118) based on the proportion of total growth achieved calculated by area within each cyclical growth mark (CGM)/maximum cross-sectional area excluding pathologic periosteal reactive bone outgrowth. Note that CGMs here refer to both lines of arrested growth (LAGs) and annuli. Colours of lines correspond to the section planes in the specimen photographs. Scale bars represent 10 cm.

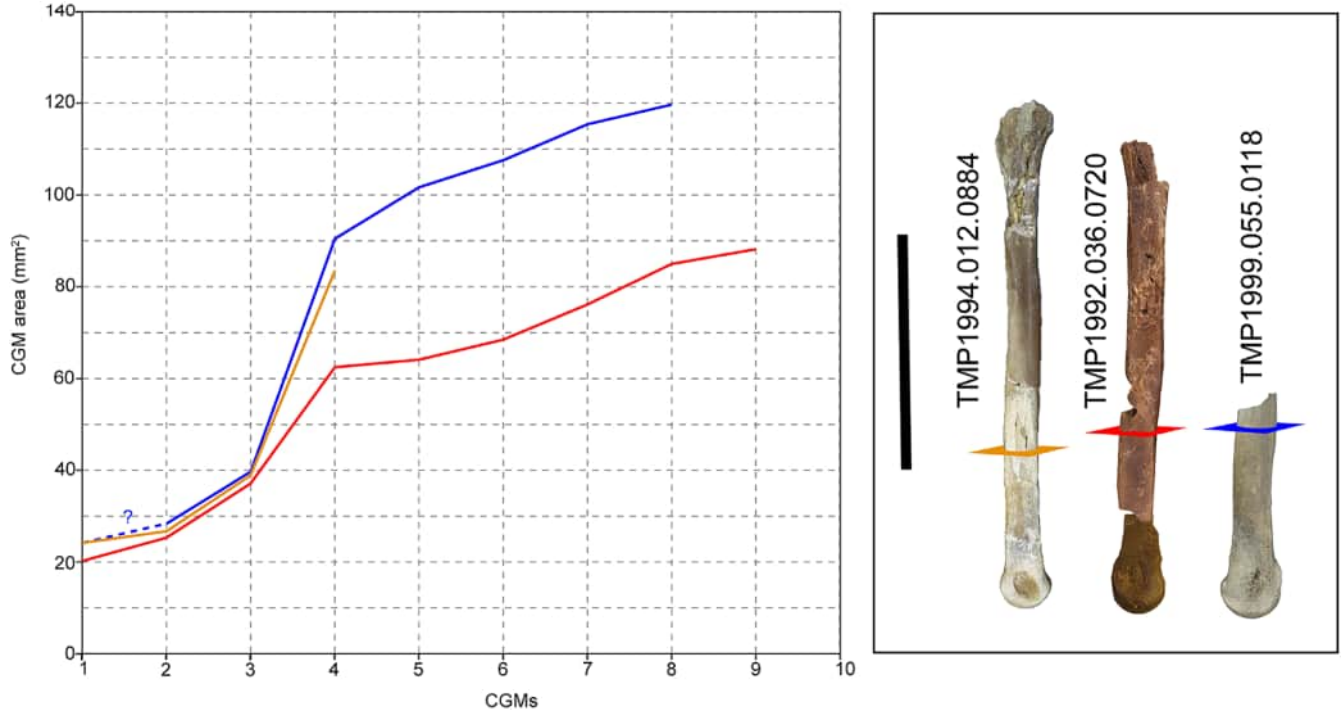

FIGURE 11 Cumulative growth graphs for metatarsal II based on measured areas within cyclical growth marks (CGMs). Colours correspond to specimen sampled. The dotted line represents unknown measurements based on missing CGM that has been destroyed by the expansion of the medullary cavity. Photographs of sampled specimens are presented in lateral view with coloured planes representing the sampling location. Scale bar = 10 cm.

but also within other taxa that are large bodied and/or fast growing such as other groups of theropods, pterosaurs (de Ricqlès et al., 2000) and derived synapsids including mammals (Chinsamy-Turan & Ray, 2012). Martin et al. (2024) proposed that for troodontids, the distribution of reticular WPCs may be associated with maturation timing. The rationale for this was an abundance of reticular growth throughout the cortex in mature yet small taxa such as *Mei long* that are interpreted as having matured quickly and deeper within the cortex of larger taxa that are thought to have matured slower but grown larger. Within our dataset, despite reticular bone being preferentially localised to the deeper cortex, there was no consistent pattern across specimens or even within individuals as to which CGMs the reticular WPC was contained within, suggesting that WPC type is likely too volatile and subject to variation based on other factors (Figures 1–5).

5.1.2 | Asymmetry of growth

The distribution of osteohistological features observed within the metatarsals suggests that these bones did not grow isometrically, and the constraints of the arctometatarsalian morphology and resulting distribution of strains influenced how they were remodelled. First, while reticular woven-parallel complexes were the most common, other types were present as well, and their distribution, rather than being consistently constrained within zones (e.g. internal vs. external cortex), was more often associated with topographic location (e.g. anterior vs. posterior). While predominantly radial WPCs were rare in the sample, long radial channels were present, most notably within the anterior and medial aspects of MTII, in the anterior–lateral aspect of the distal shaft of MTIV and in pathological regions of periosteal reactive bone (Figure 1). Radial WPCs have been found experimentally to have a higher subperiosteal accretion rate than other types in birds (de Margerie et al., 2002, 2004). A radial orientation was also found to be more common in bones prevented from experiencing mechanical loading via immobilisation compared to the controls in rats (Britz et al., 2012). This suggests that radially oriented vasculature may be associated with rapid growth in this region but its expression may be limited by mechanical constraints. The regions wherein radial channels were present in the troodontid metatarsals are all regions where greater expansion outwards is possible as they are free from the constraints of direct articulation with adjacent bones (Holtz, 1995). Furthermore, radial growth was conspicuously absent in MTIII, which lies firmly wedged between MTII and MTIV, restricting rapid outward growth. Laminar and plexiform WPCs were present as well. Occasionally, it was associated with LAGs and annuli, but it was most abundant along the medial edges of the upper-shaft sections of MTIV (Figures 1a^{I} and 5c^{II}). Given the asymmetrical shape of the troodontid metatarsus where MTIV is significantly larger than MTII and MTIII, the medial surface of MTIV along the upper half of the shaft corresponds to the central longitudinal axis of the arctometatarsus (Figure 1). This pattern of deposition may indicate a specific adaptation for load bearing in this region of the metatarsus, as laminar/circumferential vasculature has

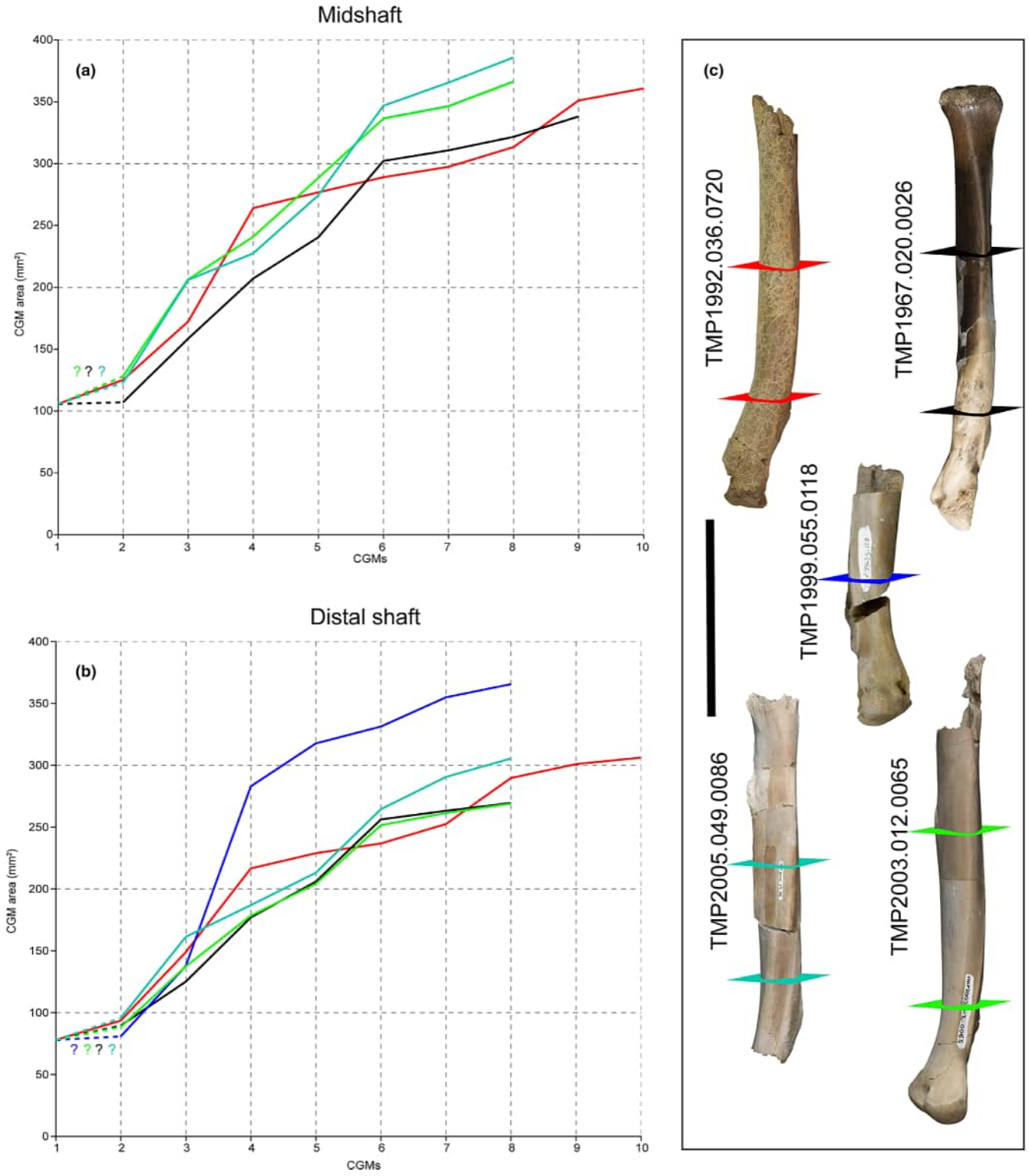

FIGURE 12 Cumulative growth graphs for metatarsal IV created by measuring the cumulative area within cyclical growth marks (CGMs). (a) Cumulative growth graphs from the midshaft region of metatarsal IV. Colours correspond to specimens and dotted lines signify unknown regions corresponding to growth following missing CGMs determined with retrocalculation. (b) Cumulative growth graphs from the distal shaft sections of metatarsal IV. Colours correspond to specimens and dotted lines signify unknown regions corresponding to growth following missing CGMs determined with retrocalculation. (c) Sampled specimens in anterior view with sections marked and colour coded to match corresponding growth lines. All specimens except TMP1999.055.0118 were sampled at the distal shaft and midshaft. Scale bar = 10 cm.

been demonstrated in the past to be a possible solution for resisting high torsional loads, for example, in bird wings (de Margerie, 2002). However, this does not explain all occurrences of this type of bone in vertebrates (Castanet et al., 1996; Main et al., 2021). Experimental studies on *Dromaius novaehollandiae* femora have also correlated laminarity with old age, larger size and slower growth (Kuehn et al., 2019). Laminarity was indeed more abundant in the largest MTIV (TMP1999.055.0118), and across specimens, it was often associated with LAGs and annuli where growth had slowed. Thus, another possibility for the concentration of laminar bone along the medial surface of the upper shaft of MTIV could simply be that it is a region that develops slower.

Another growth indicator that was regionally variable within the cortex was the EFS. This feature composed of ALB is an indicator of achieving somatic maturity and cessation of growth, and thus, its presence has been used as an indicator of reaching full maturity (Huttenlocker et al., 2013). Most specimens in the present study possessed an EFS (Table 1) but not around the entire circumference of the cortex. Instead, most of them had a partial EFS, localised along articular surfaces (medial aspect in MTIV, lateral aspect in MTII and along the entire posterior apex in MTIII) and along surfaces interpreted as entheses for tendon attachment (posterolateral apex in MTIV) (Figure 1) (George & Berger, 1966). In these specimens, the anterior surfaces and the areas opposite the articular surfaces did not have an EFS, as indicated by the presence of vascularity and developing primary osteons along the outer margin of the cortex. This lends further support to the notion that as the metatarsals grow and expand in thickness, growth ceases along entheses and articular surfaces first, but continues outwards in the regions where there is less limitation from soft tissue and other adjacent bones.

5.1.3 | Asymmetry of remodelling

Haversian bone was found in two places: intracortically where it replaced the typical woven-parallel bone and, as a result, interrupted LAGs, and within pathological periosteal reactive bone. Within the cortex, Haversian bone tissue was most common along regions with interpreted or observed tissue interactions, spanning the cortex from the endosteum to the periosteum (Cullen et al., 2014). These include surfaces that articulate with adjacent bones (medial edge of MTIV, posterior apex of MTIII and lateral edge of MTII) and areas of suspected entheses (lateral apex of MTIV that shifts posteriorly proximally) (Figure 1). This lateral apex corresponds to a ridge of bone interpreted as a site for tendon attachment of the gastrocnemius muscle (George & Berger, 1966). These regions of remodelling also correspond to the regions where growth was interpreted as terminating first. This type of intracortical remodelling occurs either to access minerals for metabolic purposes or to repair and prevent the propagation of damage, particularly microcracks (Currey, 2002; Martin, 2002; Wainwright, 1982). Given the consistency in location across individuals and its association with articulation and entheses, we interpret the functionality of the remodelling to be the latter. It is worth noting that this form of repair must be balanced against the drawback that Haversian bone is weaker during tension and bending than primary bone (Main et al., 2021). Thus, larger proximal limb elements like tibiae and femora may display more periosteal outgrowth than Haversian bone in dealing with stress, but in distal elements where lateral outgrowth and increased mass are not favourable, Haversian bone is more optimal (Cubo et al., 2015; Lieberman et al., 2003). Maintaining low mass and limiting outgrowth may be particularly important for the gracile and tightly articulated troodontid arctometatarsus.

5.2 | Interpretation of pathologies

5.2.1 | TMP1967.020.0026

In the absence of a complete individual and full three-dimensional (3D) radiological imaging, we take the most conservative approach in diagnosing pathological individuals (Figure 6). The primary pathological feature of this right MTIV is a dense, localised, slightly undulating swell of periosteal reactive bone lacking a distinct sclerotic margin. The swell is not porous and there are no signs of bone lysis or abscesses. Furthermore, both articular surfaces are preserved and are normal in appearance. Periosteal reactions like this typically result from the body's response to stress and/or injury, infection (which can also be post-traumatic) or neoplasia (tumour) (Bertozzo et al., 2024; Cruzado-Caballero et al., 2021; Kato et al., 2020; Senter & Juengst, 2016; Tanke & Rothschild, 2002; Tsogtbaatar et al., 2023). Osteomyelitis (infection of bone) is characterised by irregular and disorganised new bone growth; bone death (osteonecrosis), particularly at or near the focal point of the infection; and bone destruction (osteolysis), which can form abnormal connections/channels between the inside of the bone and the outside (called a bone fistula) and/or pockets where inflammatory cells and exudate accumulate (Huchzermeyer & Cooper, 2000; Palmer, 1992; Tsogtbaatar et al., 2023). Osteolysis is especially important for the diagnosis of osteomyelitis in reptiles and birds given that minimal periosteal reaction occurs in these groups (Grosso, 2019). The smooth, organised nature of the periosteal reactive bone and lack of erosive features preclude an infection diagnosis here. Neoplasia is also rejected as the pathology is neither sharply demarcated (seen in benign tumours) nor infiltrative or particularly destructive of the bone architecture (as in malignant tumours) (Hernandez-Divers & Garner, 2003; Krautwald-Junghanns & Schmidt, 2011; Rothschild, 2009). Therefore, we interpret this condition as stress or traumatic in origin. Fracture calluses are among the most commonly reported conditions in the paleopathology record (Tanke & Rothschild, 2002). These are characterised by rapidly growing well-vascularised primary woven bone trabeculae often described in dinosaurs as radially oriented/perpendicular to the long axis of the bone (Bertozzo et al., 2024; Griffin, 2018; Straight et al., 2009; Tsogtbaatar et al., 2023) as was exhibited here. The only problem with this diagnosis, however, is that neither gross examination nor histological assessment was able to identify

a clear fracture line. This does not necessarily preclude the diagnosis of a fracture however, as many fractures do not distort the overall shape and alignment of the bone and thus may not be obvious on gross examination, particularly in cases where the fractures are small (e.g. greenstick, stress and hairline fractures) (Bertozzo et al., 2024; Rothschild & Lambert, 2021). Additionally, the presence of a region wherein the normal primary cortical bone and growth marks are interrupted by pathological reactive bone and secondary osteons suggests localised response to damage to the primary bone cortex, indicating that perhaps the fracture occurred in that region but elsewhere along the length of the bone and was simply not clearly captured in the histological section (Figure 6b^{I}). Even in cases where high-resolution radiologic methods are used to 3D assess the entire bone, fractures may not always be visible, particularly if they have been well-healed (Bertozzo et al., 2024). Thus, we interpret TMP1967.020.0026 as presenting with a chronic stable callus secondary to a superficial cortical fracture that is well into the reparative phase of healing (as evidenced by the presence of a fully developed stable hard callus) and beginning the remodelling phase (as evidenced by the presence of a few secondary osteons within the callus region (Bigham-Sadegh & Oryan, 2015; González, 2019; Grosso, 2019; Tsogtbaatar et al., 2023)).

A differential diagnosis is that this represents periostitis (inflammation of the periosteum). This can be chronic as a result of repeated stresses or acute, resulting from localised low-grade trauma or soft tissue infection adjacent to the bone (Kealy et al., 2011; Palmer, 1992). In TMP1967.020.0026, within the periosteal reaction itself, the radial orientation and lack of grading in bone architecture from internal to external suggest that it deposited quickly over a short period of time, suggesting a more acute etiology. However, internal to the periosteal reactive bone, the appearance of a narrow lens of hypervascularised tissue within the EFS is worth noting and perhaps indicates more chronic stressors or multiple incidents disrupting the normal deposition of subperiosteal ALB (Figure 6b^{II}). However, we reject periostitis or alternative modes of abnormal periosteal bone growth on two grounds. First is the lack of erosive features produced by osteolysis and the smooth nature of the external surface of the periosteal reactive bone (not jagged or irregular) precluding an inflammatory or infectious diagnosis along or external to the periosteum. Second is the disruption of the primary bone cortex (Figure 6b^{I}), suggesting this condition was not solely external to the bone (Palmer, 1992).

Another condition previously reported in the literature that bears a striking resemblance to TMP1967.020.0026 is an ossified subperiosteal hematoma in a gorgonopsian (Kato et al., 2020). Ossified hematomas are seldom reported in the paleopathological literature and are only reported in humans in the extant pathology literature, though the condition is quite rare (Munger et al., 2021; Rajapakse & Kiddle, 2006). However, ossified hematomas are reported as having a radiological and histological presentation quite different from what was observed in Kato et al. (2020) and in TMP1967.020.0026. While ossified hematomas do show mineralisation or osseous metaplasia (bone formation) (either as a thin rim along the outside or in a central region of the lesion), the bulk of the lesion is soft tissue (blood) (Lee & Yun, 2017; Rajapakse & Kiddle, 2006). On CT imaging, this appears as a mix of hypodense and hyperdense areas corresponding with the soft tissue and mineralised regions, respectively. In cases where the ossified hematoma is subperiosteal, the periosteum is lifted away from the bone as the underlying region fills with blood; but as a result, the dystrophic mineralisation/ossification is scattered and not uniformly dense, radially oriented woven bone, as was seen in this specimen (Lee & Yun, 2017). Therefore, given the features observed here and the lack of cases reported in the modern veterinary literature, we reject a diagnosis of a subperiosteal ossified hematoma for TMP1967.020.0026 and the gorgonopsian in Kato et al. (2020). Regardless of diagnosis, the gross morphology of TMP1967.020.0026 was very subtle, and there may be other specimens with superficially unremarkable features in collections that have been missed. Not every trauma is going to be visually obvious on gross examination, so we may be vastly underreporting the occurrence of injuries even in well-studied taxa.

5.2.2 | TMP2005.049.0086

Unlike the previous specimen, the pathology on this partial right MTIV presents some different characteristics (Figure 7). Rather than a relatively smooth dense mass, this bony outgrowth was a smaller bony spur with a more irregular, bumpy and porous texture on gross morphological examination. It was also located more proximally, along the posterolateral ridge of the metatarsal shaft. On gross examination, this pathology most strongly resembles osteophytes and enthesophytes, which are common in the paleopathology record (Anné et al., 2016; Bell, 2010; Gonzalez et al., 2017; Tschopp et al., 2014). The difference between these conditions is the location. Osteophytes occur along joint margins and thus in long bones are localised along the margins of articular surfaces, whereas enthesophytes form at the entheses of tendons and ligaments (Benjamin et al., 2006; Palmer, 1992) These bumps of new bone form on the surface of pre-existing bone and have been associated with a variety of conditions including trauma, but most commonly from either a single injury or repeated minor injuries to the periosteum in a localised area (such as an enthesis) (Benjamin et al., 2006; Palmer, 1992). For this specimen, the location of the pathology corresponds to the proposed tendon insertion site for the gastrocnemius pars lateralis muscle. While a full muscle reconstruction for the hindlimbs of troodontids has not yet been done, we base our assessment on the positioning of this muscle in birds (George & Berger, 1966) and the interpretation of muscle scarring on the long bones in non-avian theropods (Carrano & Hutchinson, 2002; Hutchinson, 2002). Additionally, another specimen in our dataset, TMP2003.012.0065, preserves a subtle undulating texture corresponding to the same region as the pathology on TMP2005.049.0086 that did not appear pathologic on histological analysis but is instead interpreted as muscle scarring, thus, supporting the presence of tendon activity in this region.

Histological analysis provides a little bit more insight into the nature of this pathology by revealing a network of woven-fibered trabeculae oriented primarily laterally, but with some oriented posteriorly as well, perhaps suggesting two or more different directional stressors pulling on the bone surface or chronic stress in the region (Figure 7b[I]). Additionally, and more importantly, however, is the disruption of the primary bone cortex similar to what was seen in TMP1967.020.0026 (Figures 6 and 7b[I]) and the subtle swell of periosteal reactive bone that extends anteriorly and distally from the focal point of the pathology (Figures 4b, 5b and 7b[II]). This periosteal reaction resembles a chronic stable callus in the remodelling phase of healing containing radially and longitudinally oriented primary osteons within a scaffolding of woven-fibered trabeculae but limited secondary osteons. Towards the outside in some regions, layers of ALB can also be seen suggesting periods of slower growth following the deposition of some of the pathological bone (Figure 7b[I]). Extensive callus formation and disturbance of the primary bone cortex are not characteristic of enthesophytes, and therefore, we interpret these features as representing an avulsion or chip fracture and associated chronic callus formation that may or may not have begun as an enthesophyte. Avulsion and chip fractures occur when the pull of a ligament or tendon dislodges a small piece of bone suggesting a localised stress-based traumatic origin for the pathology seen here (Aithal et al., 2023; Grosso, 2019; Palmer, 1992). In cursorial birds like the emu (*D. novaehollandiae*), wherein much of the running stride comes from the lower leg, the gastrocnemius, which is responsible for plantarflexion, is one of the most important running muscles (Patak & Baldwin, 1993). The combination of a tightly articulated and long arctometatarsus in troodontids resulting in a proportionally longer lower hindlimb suggests they also had high potential for cursoriality (Persons & Currie, 2016). Thus, a stress-related injury from extended activity of the gastrocnemius is not unexpected.

5.2.3 | TMP1992.036.0720

The pathological features on this specimen were the most extensive and the most perplexing. Both elements preserved for this individual display abnormalities but to differing degrees (Figures 8 and 9). MTIV was the most extensively pathologic. Along the shaft, periosteal reactive bone of radial woven-fibered trabeculae suggests chronic callus formation, as was seen in TMP1967.020.0026 and TMP2005.049.0086 (Figure 9). However, instead of being localised, the periosteal reactive bone growth extends along the length of the shaft and varies in density and extent of remodeling throughout the length of the shaft (Figure 8). Notable as well is the presence of distinct regions demarcated by LAGs within some areas of the periosteal reaction (Figure 9b[I],c[II]). These differences suggest that the pathology was not a simple acute incident but rather multiple incidents or chronic stressors sustained over at least an entire growth season, permitting different degrees of healing throughout. Furthermore, unlike the other specimens, split LAGs within the normal primary bone cortex are abundant in this individual in both MTII and MTIV (Figures 2b and 9a[III]). These are thought to have occurred within one growth season and are attributed to environmental stressors (Cullen, Brown, et al., 2021; Francillon-Vieillot et al., 1993), thus providing further evidence that stressors were pervasive in this animal's life and could represent an earlier sign of pathology predating the deposition of the periosteal reactive bone, especially considering its presence in both elements. The distal end of the MTIV provides the most clues as to possible etiology. Unlike the other two pathological specimens, this one features extensive disorganised bone lysis, as much of the distal end appears eaten away resulting in deeper, irregular ligament pits (Figure 8c,e), and a misshapen and reduced articular surface featuring pitting resembling subchondral cysts (Figure 8f). The distal end of MTII seems relatively normal, but it is worth noting that this element is not a primary weight-bearing bone in Troodontidae (Russell, 1969), which may preclude it from developing certain pathologies. Given the chronic callus formation and distal-end erosive features observed in MTIV, we propose a traumatic injury to the foot but particularly to the distal region of MTIV causing a chronic inflammatory cascade that resulted in osteolysis and ulcerative lesions to the articular surface and additional bone proliferation. While fractures were not visible on gross morphological examination, small ones may be visible within the primary bone cortex of the distal-most histological section (Figure 9a[I]). However, full radiological examination would be recommended for better assessment and confirmation of their identity. If damage occurred sufficiently early in the animal's life, it is also possible that remodelling has obliterated evidence of prior damage.

A differential diagnosis for the features seen here is a form of degenerative articular disease (arthropathy) or arthritis. Arthropathy (sometimes referred to as osteoarthritis, degenerative joint disease or degenerative osteoarthritis) is defined by its degenerative nature, and it can be primary or occur secondary to developmental, nutritional or traumatic causes (Palmer, 1992). In arthropathy, chronicity can lead to deterioration of the joint surface, formation of osteophytes and eburnation of the subchondral bone (a process wherein the bone surface becomes dense and polished in response to cartilage loss and bone-on-bone friction). While considered rare in wild extant mammals and reptiles, arthropathy has been reported numerous times in domestic species and captive populations, though it is usually found incidentally, which suggests that it may simply be under-sampled and under-studied in wild individuals (Degernes et al., 2011; Grosso, 2019; Hartup et al., 2018; Rothschild, 1990, 2010; Sokoloff, 1959). Arthritis, conversely, is primarily inflammatory in nature and can be subdivided into infectious and non-infectious, the latter of which is usually caused by some form of immunological disturbance (e.g. rheumatoid arthritis in humans) (Majithia & Geraci, 2007; Palmer, 1992). In birds and reptiles, infections of the bones and joints are typically more localised than in mammals, and while bone proliferation along the joint margins is a feature for infectious forms of arthritis in these

taxa, osteolysis is the dominant characteristic (Anné et al., 2016; Grosso, 2019; Stacy & Pessier, 2007; Williams, 2002). As far as we are aware, immunological forms of arthritis have not been previously described for non-mammals. In mammals, however, it is typically symmetric, presenting with bilateral osteophytes, and affects multiple joints (Palmer, 1992). Despite presenting with extensive osteolysis characteristic of chronic inflammation and secondary proliferative periosteal bone growth, we a reject a diagnosis of joint disease in TMP1992.036.0720. Arthrosis and arthritis are terms reserved for conditions that are primarily of the joint, and despite the osseous features observed here that often occur secondarily to joint disease, without preservation of synovial or cartilaginous tissue, we cannot attribute joint disease as the primary cause. Secondly, the presence of chronic stable calluses in different stages of density and healing throughout the length of the shaft suggests that damage to the primary bone cortex was involved in producing the suite of features observed. It is still possible that arthrosis secondary to early trauma predisposed this individual to lameness and weakening of bone resulting in subsequent fractures, but if that were the case, we may expect to see eburnation at the distal articular surface of the bone (Grosso, 2019; Palmer, 1992). While eburnation does not appear present on gross examination, further analysis via radiological imaging might reveal whether subchondral sclerosis associated with eburnation was present (Li et al., 2013).

Regardless of the specific etiology, given the highly unusual articular surface of MTIV, it is likely the first phalanx of digit IV was also impacted, and the abnormal growth of MTII also suggests that whatever the cause may have been, it likely impacted much of the pes, not just MTIV and MTII. However, without more of this individual, particularly elements that directly articulate with MTII and MTIV, we cannot narrow down a diagnosis with more certainty beyond a traumatic injury resulting in chronic inflammation leading to osteolysis and reactive bone formation. The features on TMP1992.036.0720 suggest that it had the most chronic and widely impacting pathology among the sampled specimens, and its concentration on a primary weight-bearing joint may have impacted its mobility. Despite this, the individual managed to survive for some time, and the extent of healing and even deposition of LAGs within some of the periosteal reaction suggest that it had time to heal, although the process was still active at the time of the animal's death.

5.3 | Assessment of ontogenetic stages

Following the categories proposed by Martin et al. (2024), a variety of ontogenetic stages were present in our dataset. Firstly, none of the troodontid metatarsals lacked zonation. Even the smallest specimens in the sample (TMP1994.012.0884, TMP1998.068.0090 and TMP2005.049.0015) had at least two zones. However, that does not necessarily preclude juvenile status. Indeed, the appearance of these zones and how they differ, if at all, is an important factor as well. Of the small troodontid metatarsals, TMP1994.012.0884 (MTII) (section 94II-1; Figure 2a) and TMP1998.068.0090 (MTIII) (Figure 3a) exhibit a change from reticular vasculature to sub-plexiform after zone 1. However, these specimens do not display other telltale markers of slower growth towards the periosteum one would expect in a subadult, and TMP1998.068.0090 (MTIII) only has two zones, so we are tentatively referring to both specimens as juveniles. For TMP2005.049.0015 (MTIII), most variation observed was regional (i.e. differences between lateral and medial apices of the section rather than between the inner cortex and outer cortex). However, some decreased vascularity and increased presence of PFB were evident near the periosteum, suggesting growth had begun to slow down (Figure 3c). Given the poor quality of the section, however, we cannot confidently ascribe a growth stage to this specimen. Noticeable shifts in bone microanatomy from endosteum towards periosteum from faster-growing bone towards slower-growing bone have been interpreted by previous authors as an indicator of sexual maturity (Gianechini et al., 2018; Martin et al., 2024; Shen, Zhao, et al., 2017). However, using qualitative markers like this as an indicator of sexual maturity is still tenuous and not widely used. As far as histological markers are concerned, a sudden decrease in the spacing between growth marks/decrease in zone thickness is much more widely referenced as indicative of sexual maturity (Andrews, 1982; Gianechini et al., 2018; Martin et al., 2024; Shen, Zhao, et al., 2017; Shine & Charnov, 1992). Histology of brooding troodontids and oviraptorids has demonstrated sexual maturity occurring in specimens where a marked decrease in the spacing of CGMs has occurred, but somatic maturity has not yet been reached (Erickson et al., 2007). However, this is still merely an association, and no dinosaur histological study has yet devised a more precise means of pinpointing when exactly along the growth curve sexual maturity occurs. Regardless of whether it represents sexual maturity, an abrupt decrease in growth mark spacing and subsequent plateau where growth marks begin to appear closely packed together in the periosteal cortex has often been interpreted as a subadult characteristic. Most of the individuals in this study fall into this category wherein growth has slowed but not yet ceased completely (Table 1). This is not unexpected, and indeed, it has been noted by Erickson (2005) that most dinosaur specimens in museum collections are not full-sized adults (Martin et al., 2024). In specimens that have reached full somatic maturity, we would expect the presence of an EFS along the entire perimeter of the cortex. As stated previously, the EFS was found to deposit asymmetrically and was regional in most specimens, suggesting that they were late subadults or adults that were not completely finished with growth. Only two specimens (MTIV TMP1967.020.0026 and MTII, and MTIV TMP1992.036.0720) possessed a full EFS in some of their sections (Table 1) but not across all sections. This, coupled with the fact that both are pathologic, makes it difficult to conclusively state whether these specimens have indeed finished growing. Only two individuals in the study have clear growth marks but without any abrupt decrease in zone thickness (MTII

TMP1994.012.0884, MTIII TMP1998.068.0090) and are thus interpreted as juveniles. The MTIII TMP2005.049.0015 may also be a juvenile, but tracing growth markers through the cortex of this individual was difficult, precluding a clear assessment of the ontogenetic stage.

5.4 | A note on the IFS

Another growth indicator that has been used in the past by some authors to indicate a specimen is not a juvenile is the presence of an ICL/IFS (Martin et al., 2024 and references within). Because this is a secondary structure, we would expect it to be absent in juveniles below a certain age, but unlike the EFS, it is not dependent on a specific growth stage or the local rate of skeletal growth (de Buffrénil & Quilhac, 2021). Still, given the presence of an IFS in most sampled troodontids, including all specimens in the present study and juveniles, it likely develops very early. Indeed, the only troodontid ever reported lacking an IFS is a small *Troodon* femur (MOR 246), interpreted as being from a mid-term embryo based on calculated egg volume (Horner et al., 2001). There were no specimens in the present sample lacking an IFS, indicating none of them were young enough to have not yet developed one.

5.5 | Growth dynamics

As previous studies have demonstrated, osteohistology can vary considerably between different bones of an individual in multiple ways, including the number and spacing of CGMs (Cullen, Brown, et al., 2021; Cullen, Simon, et al., 2021; Martin et al., 2024; Prondvai et al., 2018). This is in part owing to allometric growth of the skeleton and the varying demands different parts of the body undergo (Prondvai et al., 2018). This can create problems when comparing multiple specimens together for constructing growth curves, as different elements or even segments from different regions along the same element can vary. By comparing the growth between MTII and IV within an individual with associated elements (TMP1992.036.0720, TMP1999.055.0118), we were able to demonstrate that the different metatarsals grew at the same rate (Figure 10). Thus, we could reasonably assume that MTII and MTIV from different individuals could be directly compared with one another. Therefore, differences in growth trajectories observed between different elements were assumed to have resulted from factors other than simply allometric growth. The most intriguing result observed was the presence of two different growth trajectories among the sampled metatarsals. Trajectory 1 (seen in TMP1994.012.0884, TMP1999.055.0118 and the early growth of TMP.1992.036.0720) (Figures 11 and 12) was characterised by the largest growth spurt occurring between the third and fourth CGM, followed by an abrupt drop in growth. It is worth noting that TMP1992.036.0720, the most pathological specimen in the present study, had a shallower growth than the other two examples, but still conforms to the overall pattern of growth trajectory 1. Conversely, trajectory 2 (TMP1967.020.0026, TMP2003.012.0065 and TMP2005.049.0086) followed a more linear growth with more evenly spaced CGMs up until the sixth wherein growth slows and plateaus (Figure 12). With the exception of the pathological TMP1992.036.0720, which appears to follow trajectory 1 but through apparent stunting resulted in a size more consistent with trajectory 2, trajectory 1 appears to correspond to a slightly larger size than trajectory 2, with TMP1999.055.0118 being ~109% the circumference and ~119% the cross-sectional area of the next largest MTIV with the same number of LAGs (TMP2005.049.0086) (Table 1). It is difficult to say how much this difference would translate to a difference in overall body size, especially given that body mass estimates are typically done with femoral proportions, so we refrain from making any conclusions based on size alone (Campione et al., 2014; Currie, 2003). More notable is the difference in timing (relative to CGM count) of the growth plateau between the two growth trajectories. If a sudden decrease in bone deposition corresponds to the onset of sexual maturity, as has been suggested previously, then half the sampled metatarsals (trajectory 1) reach sexual maturity earlier than the other half (trajectory 2). The reason for this discrepancy is uncertain. One possibility is it may indicate sexual dimorphism, as sexually dimorphic size, as well as age-to-sexual maturation dimorphism within species, is common in nature, including birds (Ancona et al., 2020). However, whether earlier sexual maturation and/or larger size would indicate male or female cannot be known given how variable dimorphism indicators between taxa can be.

Another possibility, regardless of whether the different growth trajectories indeed correspond to different maturation timing, is a taxonomic signal. Across previously assessed troodontid material, multiple growth trajectories and rates of achieving somatic maturity have been observed. However, none have been histologically sectioned in MTII or MTIV except the MTII of *Tamarro insperatus*, which does not present with any visible growth lines, precluding direct comparison (Martin et al., 2024; Sellés et al., 2021). With that in mind, trajectory 1 observed here appears most similar to MTIII of *Troodon* sp. (Varricchio, 1993), wherein specimens were described as reaching adult size in 3–5 LAGs. Trajectory 2, on the other hand, is most similar to the fibula of *T. sampsoni*, where growth decrease was occurring at around LAG 5–6 (Zanno et al., 2011). Multiple species of small carnivores and mesocarnivores from the same family occupying the same environment is a common occurrence in extant ecosystems (e.g. multiple species of canids and felids co-occuring in sub-Saharan African savannah ecosystems) (Castelló, 2018, 2020). Given the fossil record likely underestimates species diversity (Flannery Sutherland et al., 2019), it is not unreasonable to suspect we are missing diversity even in a well-sampled system such as the DPF (Brown et al., 2013). Indeed, the presence of more than one troodontid inhabiting the DPF has been proposed in the past, but without overlapping diagnostic material, and both proposed species bearing considerable stratigraphic overlap, that designation has remained tenuous (Cullen, Zanno, et al., 2021; van der Reest & Currie, 2017). Given limited detailed stratigraphic information and

good diagnostic features for the specimens in the present study, we cannot make any further claims on the taxonomic identity of the troodontids in the DPF other than the possibility that there may be more than one. Further histological study of specimens, particularly articulated and/or with associated diagnostic material, may provide better insights, and indeed, we recommend that histological sampling should be incorporated into more descriptive studies, particularly in cases where long weight-bearing bones are preserved to allow for another point of comparison with the existing material.

5.6 | Impact of pathologies on growth

When studying the life histories of animals, it is important to consider variables that may cause deviations from the norm. The inclusion of pathological individuals provided an opportunity for direct comparison with healthy normal growth. For MTIV TMP1967.020.0026 and MTIV TMP2005.049.0086, their growth trajectories remain similar to each other and to the healthy MTIV TMP2003.012.0065 (trajectory 2), suggesting that the pathologies incurred did not significantly affect the growth of the animals (Figure 12). Both pathologies are interpreted as localised responses to trauma and stress and thus would likely not have impacted the growth of the bone or the organism overall over its lifetime. This is especially the case if the pathologies occurred later in life. TMP1992.036.0720, on the other hand, follows growth trajectory 1 and thus exhibits a growth spurt from CGM 3 to 4, but it is suppressed compared to the other individuals. It is worth noting as well that the timing of major steps within the growth trajectory (i.e. when the growth spurts and plateau occur) does not appear to be affected, but rather the extent to which the animal is able to deposit new bone. The fact that both the preserved elements for this individual (MTII and MTIV) exhibit this and both show signs of pathology suggests that perhaps the condition(s) experienced by this individual are more widespread and chronic and may have hindered the growth of the individual. Without the rest of the elements of the foot, it is impossible to say how widespread the abnormalities were, but given that both were affected throughout the length of the bone and MTIV was affected heavily on the distal articular surface suggests that at least MTIII and the first phalanx of digit IV may have shown irregularities as well. While the diagnosis for this individual is uncertain, the unusual growth demonstrated in comparison to the other pathological individuals also lends support to a more complex and chronic disease etiology as opposed to a simple well-healed acute insult. Additionally, the variable presentation of the periosteal reactive bone throughout the shaft of MTIV and the presence of apparent LAGs within them separating the periosteal reactive bone into distinct layers suggest that the pathologies may have occurred over an extended period of time (Figure 9). Thus, despite the extent of pathology, TMP1992.036.0720 may have lived with the condition and survived for some time before death. By sampling a variety of specimens, including multiple pathological individuals, we show here that the effects of pathology on growth trajectories are variable and may be dependent on diagnosis and when the animal was affected. When studying specimens histologically, it is thus important to keep in mind the health of the individual and use comparative healthy material as a reference when possible, especially if pathologies are extensive.

6 | CONCLUSIONS

In the absence of abundant or complete material as is the case with North American troodontids, reconstructing life histories can be difficult. Histological surveys are thus a valuable tool for extracting new data from available material, even isolated bones that may not be as informative on their own. Isolated metatarsals are among the most commonly recognised troodontid bones from the DPF. Histological sectioning reveals that within the cortex, the metatarsals grew and remodelled asymmetrically, ceasing growth and depositing an EFS first along the articular surfaces and entheses where remodelling via secondary osteons is also concentrated. Meanwhile, they continued to deposit more bone anteriorly and opposite the articular surfaces where there is greater room for expansion free from the constraints of the tightly articulated arctometatarsus. Here we also describe three pathological metatarsals, the first pathological troodontid elements to be histologically assessed. Two of the individuals present with relatively localised conditions. The first is a chronic stable callus in response to a superficial cortical fracture, while the second appears to be a minor avulsion or chip fracture arising from stress at the posterolateral insertion site of the gastrocnemius. Conversely, one of the specimens (TMP1992.036.0720) presented with a myriad of abnormalities that suggest a traumatic event or series of events affecting the pes more broadly, resulting in chronic callus formation throughout the shaft and chronic inflammation at the distal joint of MTIV, and deformation of MTII. However, the precise etiology of this condition is still uncertain, and further study with additional imaging may be necessary for a more accurate diagnosis. Regardless, the growth of these specimens in comparison with other healthy individuals revealed the presence of at least two growth trajectories within the DPF, but whether they represent sexual, taxonomic or other signals is unknown and warrants further study and better specimens. Pathology can be ruled out as the sole reason for the presence of these growth trajectories, as only the growth of TMP1992.036.0720 appeared to have been impacted by pathology. This suggests that acute and/or localised injuries to the bone surface, particularly occurring later in life, are expected to have negligible effects on the overall growth of the animal, but more widespread and chronic conditions, particularly if they commenced earlier in development, could impact the extent of growth an animal is able to achieve.

AUTHOR CONTRIBUTIONS

CWG led the study. PJC provided project administration. CWG and MJP conceptualised the study. CWG, MJP and ADD conducted data collection. CWG, MJP and ADD conducted data analysis. CWG wrote the original draft and created figures. MJP, ADD and PJC

supervised the project. All authors provided valuable insights, comments and feedback for improving the study.

ACKNOWLEDGEMENTS

We would like to thank Yan-Yin Wang for technical assistance with 3D scanning and histological sectioning, Michael Caldwell for providing access to microscope and imaging facilities and Corwin Sullivan for allowing access to 3D scanning facilities and software. Henry Sharpe, Kyla Beguesse and Annie McIntosh provided helpful discussion and support. Brandon Strilisky, Tom Courtenay and Jillian Richard (TMP) are thanked for specimen access and for providing permission for destructive sampling. We also thank the two anonymous reviewers for their helpful comments that improved this manuscript.

CONFLICT OF INTEREST STATEMENT

We have no conflicts of interest to declare.

DATA AVAILABILITY STATEMENT

Data available in article Supporting Information.

ORCID

Christiana W. Garros https://orcid.org/0000-0001-8049-6269

REFERENCES

Aithal, H.P., Pal, A., Kinjavdekar, P. & Pawde, A.M. (2023) Basic considerations. In: Aithal, H.P., Pal, A., Kinjavdekar, P. & Pawde, A.M. (Eds.) *Textbook of veterinary Orthopaedic surgery*. New York, NY: Springer, pp. 1–60.

Ancona, S., Liker, A., Carmona-Isunza, M.C. & Székely, T. (2020) Sex differences in age-to-maturation relate to sexual selection and adult sex ratios in birds. *Evolution Letters*, 4(1), 44–53. Available from: https://doi.org/10.1002/evl3.156

Andrews, R.M. (1982) Patterns of growth in reptiles. In: Gans, C. & Pough, F.H. (Eds.) *Biology of the Reptilia*, Vol. 13. New York, NY: Academic Press, pp. 273–320.

Anné, J., Hedrick, B.P. & Schein, J.P. (2016) First diagnosis of septic arthritis in a dinosaur. *Royal Society Open Science*, 3(8), 160222.

Bell, P.R. (2010) Palaeopathological changes in a population of *Albertosaurus sarcophagus* from the upper cretaceous horseshoe canyon formation of Alberta, Canada. *Canadian Journal of Earth Sciences*, 47(9), 1263–1268.

Benjamin, M., Toumi, H., Ralphs, J.R., Bydder, G., Best, T.M. & Milz, S. (2006) Where tendons and ligaments meet bone: attachment sites ('entheses') in relation to exercise and/or mechanical load. *Journal of Anatomy*, 208(4), 471–490.

Bertozzo, F., Stein, K., Varotto, E., Galassi, F.M., Ruffell, A. & Murphy, E. (2024) Histological analysis and etiology of a pathological iguanodontian femur from England. *Journal of Anatomy*, 245(3), 490–500.

Bigham-Sadegh, A. & Oryan, A. (2015) Basic concepts regarding fracture healing and the current options and future directions in managing bone fractures. *International Wound Journal*, 12(3), 238–247.

Britz, H.M., Jokihaara, J., Leppänen, O.V., Järvinen, T.L. & Cooper, D.M. (2012) The effects of immobilization on vascular canal orientation in rat cortical bone. *Journal of Anatomy*, 220(1), 67–76. Available from: https://doi.org/10.1111/j.1469-7580.2011.01450.x

Brown, C.M., Campione, N.E., Mantilla, G.P.W. & Evans, D.C. (2022) Size-driven preservational and macroecological biases in the latest Maastrichtian terrestrial vertebrate assemblages of North America. *Paleobiology*, 48(2), 210–238. Available from: https://doi.org/10.1017/pab.2021.35

Brown, C.M., Evans, D.C., Campione, N.E., O'Brien, L.J. & Eberth, D.A. (2013) Evidence for taphonomic size bias in the Dinosaur Park formation (Campanian, Alberta), a model Mesozoic terrestrial alluvial-paralic system. *Palaeogeography, Palaeoclimatology, Palaeoecology*, 372, 108–122.

Campione, N.E., Evans, D.C., Brown, C.M. & Carrano, M.T. (2014) Body mass estimation in non-avian bipeds using a theoretical conversion to quadruped stylopodial proportions. *Methods in Ecology and Evolution*, 5(9), 913–923.

Carrano, M.T. & Hutchinson, J.R. (2002) Pelvic and hindlimb musculature of *Tyrannosaurus rex* (Dinosauria: Theropoda). *Journal of Morphology*, 253(3), 207–228. Available from: https://doi.org/10.1002/jmor.10018

Castanet, J., Croci, S., Aujard, F., Perret, M., Cubo, J. & de Margerie, E. (2004) Lines of arrested growth in bone and age estimation in a small primate: *Microcebus murinus*. *Journal of Zoology*, 263(1), 31–39.

Castanet, J., Grandin, A., Abourachid, A. & de Ricqlès, A. (1996) Expression of growth dynamic in the structure of periosteal bone in *Anas platyrhynchos*. *Comptes Rendus de l'Academie des Sciences. Serie III, Sciences de la Vie*, 319(4), 301–308.

Castelló, J.R. (2018) *Canids of the world: wolves, wild dogs, foxes, jackals, coyotes, and their relatives*. Princeton, NJ: Princeton University Press.

Castelló, J.R. (2020) *Felids and hyenas of the world: wildcats, panthers, lynx, pumas, ocelots, caracals, and relatives*. Princeton, NJ: Princeton University Press.

Chinsamy-Turan, A.A.S.R. & Ray, S. (2012) Bone histology of some therocephalians and gorgonopsians, and evidence of bone degradation by fungi. In: Chinsamy-Turan, A. (Ed.) *Forerunners of mammals: radiation, histology, biology*. Bloomington, IN: Indiana University Press, pp. 199–222.

Cruzado-Caballero, P., Díaz-Martínez, I., Rothschild, B., Bedell, M. & Pereda-Suberbiola, X. (2021) A limping dinosaur in the late Jurassic: pathologies in the pes of the neornithischian *Othnielosaurus consors* from the Morrison formation (Upper Jurassic, USA). *Historical Biology*, 33(9), 1753–1759. Available from: https://doi.org/10.1080/08912963.2020.1734589

Cubo, J., Woodward, H., Wolff, E. & Horner, J.R. (2015) First reported cases of biomechanically adaptive bone modeling in non-avian dinosaurs. *PLoS One*, 10(7), e0131131.

Cullen, T.M., Brown, C.M., Chiba, K., Brink, K.S., Makovicky, P.J. & Evans, D.C. (2021) Growth variability, dimensional scaling, and the interpretation of osteohistological growth data. *Biology Letters*, 17(11), 20210383.

Cullen, T.M., Canale, J.I., Apesteguía, S., Smith, N.D., Hu, D. & Makovicky, P.J. (2020) Osteohistological analyses reveal diverse strategies of theropod dinosaur body-size evolution. *Proceedings of the Royal Society B*, 287(1939), 20202258.

Cullen, T.M. & Cousens, B.L. (2024) New biogeochemical insights into Mesozoic terrestrial paleoecology and evidence for omnivory in troodontid dinosaurs. *Geological Society of America Bulletin*, 136(7–8), 2689–2701.

Cullen, T.M., Evans, D.C., Ryan, M.J., Currie, P.J. & Kobayashi, Y. (2014) Osteohistological variation in growth marks and osteocyte lacunar density in a theropod dinosaur (Coelurosauria: Ornithomimidae). *BMC Evolutionary Biology*, 14, 1–14.

Cullen, T.M., Simon, D.J., Benner, E.K. & Evans, D.C. (2021) Morphology and osteohistology of a large-bodied caenagnathid (Theropoda, Oviraptorosauria) from the Hell Creek formation (Montana): implications for size-based classifications and growth reconstruction in theropods. *Papers in Palaeontology*, 7(2), 751–767. Available from: https://doi.org/10.1002/spp2.1302

Cullen, T.M., Zanno, L., Larson, D.W., Todd, E., Currie, P.J. & Evans, D.C. (2021) Anatomical, morphometric, and stratigraphic analyses

of theropod biodiversity in the upper cretaceous (Campanian) Dinosaur Park formation. *Canadian Journal of Earth Sciences*, 58(9), 870–884.

Currey, J.D. (2002) *Bones: structure and mechanics*. Princeton, NJ: Princeton University Press.

Currie, P.J. (1985) Cranial anatomy of *Stenonychosaurus inequalis* (Saurischia, Theropoda) and its bearing on the origin of birds. *Canadian Journal of Earth Sciences*, 22(11), 1643–1658. Available from: https://doi.org/10.1139/e85-173

Currie, P.J. (2003) Allometric growth in tyrannosaurids (Dinosauria: Theropoda) from the upper cretaceous of North America and Asia. *Canadian Journal of Earth Sciences*, 40(4), 651–665.

de Buffrénil, V. & Castanet, J. (2000) Age estimation by skeletochronology in the Nile monitor (*Varanus niloticus*), a highly exploited species. *Journal of Herpetology*, 34(3), 414–424. Available from: https://doi.org/10.2307/1565365

de Buffrénil, V. & Quilhac, A. (2021) Bone tissue types: a brief account of currently used categories. In: de Buffrénil, V., Ricqlès, A.J., Zylberberg, L. & Padian, K. (Eds.) *Vertebrate skeletal histology and paleohistology*. Boca Raton, FL: CRC Press, pp. 147–190.

de Margerie, E. (2002) Laminar bone as an adaptation to torsional loads in flapping flight. *Journal of Anatomy*, 201(6), 521–526.

de Margerie, E., Cubo, J. & Castanet, J. (2002) Bone typology and growth rate: testing and quantifying 'Amprino's rule' in the mallard (*Anas platyrhynchos*). *Comptes Rendus Biologies*, 325(3), 221–230.

de Margerie, E.D., Robin, J.P., Verrier, D., Cubo, J., Groscolas, R. & Castanet, J. (2004) Assessing a relationship between bone microstructure and growth rate: a fluorescent labelling study in the king penguin chick (*Aptenodytes patagonicus*). *Journal of Experimental Biology*, 207(5), 869–879. Available from: https://doi.org/10.1242/jeb.00841

de Ricqlès, A.D. (1980) Tissue structures of dinosaur bone, functional significance and possible relation to dinosaur physiology. A Cold Look at the Warm-Blooded Dinosaurs, 103–139.

de Ricqlès, A.J., Padian, K., Horner, J.R. & Francillon-Vieillot, H. (2000) Palaeohistology of the bones of pterosaurs (Reptilia: Archosauria): anatomy, ontogeny, and biomechanical implications. *Zoological Journal of the Linnean Society*, 129(3), 349–385. Available from: https://doi.org/10.1111/j.1096-3642.2000.tb00016.x

Degernes, L.A., Lynch, P.S. & Shivaprasad, H.L. (2011) Degenerative joint disease in captive waterfowl. *Avian Pathology*, 40(1), 103–110.

Enlow, D.H. (1963) Principles of bone remodeling: an account of post-Natal growth and remodeling processes in long bones and the mandible. *Medical Journal of Australia*, 2, 906.

Erickson, G.M. (2005) Assessing dinosaur growth patterns: a microscopic revolution. *Trends in Ecology & Evolution*, 20(12), 677–684.

Erickson, G.M., Curry Rogers, K., Varricchio, D.J., Norell, M.A. & Xu, X. (2007) Growth patterns in brooding dinosaurs reveals the timing of sexual maturity in non-avian dinosaurs and genesis of the avian condition. *Biology Letters*, 3(5), 558–561.

Erickson, G.M., Rauhut, O.W., Zhou, Z., Turner, A.H., Inouye, B.D., Hu, D. et al. (2009) Was dinosaurian physiology inherited by birds? Reconciling slow growth in *Archaeopteryx*. *PLoS One*, 4(10), e7390. Available from: https://doi.org/10.1371/journal.pone.0007390

Evans, D.C., Barrett, P.M., Brink, K.S. & Carrano, M.T. (2015) Osteology and bone microstructure of new, small theropod dinosaur material from the early late cretaceous of Morocco. *Gondwana Research*, 27(3), 1034–1041. Available from: https://doi.org/10.1016/j.gr.2014.03.016

Evans, D.C., Cullen, T.M., Larson, D.W. & Rego, A. (2017) A new species of troodontid theropod (Dinosauria: Maniraptora) from the horseshoe canyon formation (Maastrichtian) of Alberta, Canada. *Canadian Journal of Earth Sciences*, 54(8), 813–826. Available from: https://doi.org/10.1139/cjes-2017-0034

Fiorillo, A.R. (2008) On the occurrence of exceptionally large teeth of *Troodon* (Dinosauria: Saurischia) from the late cretaceous of northern Alaska. *PALAIOS*, 23(5), 322–328.

Flannery Sutherland, J.T., Moon, B.C., Stubbs, T.L. & Benton, M.J. (2019) Does exceptional preservation distort our view of disparity in the fossil record? *Proceedings of the Royal Society B: Biological Sciences*, 286(1897), 20190091.

Fowler, D.W., Freedman, E.A., Scannella, J.B. & Kambic, R.E. (2011) The predatory ecology of *Deinonychus* and the origin of flapping in birds. *PLoS One*, 6(12), e28964.

Francillon-Vieillot, H., de Buffrénil, V., Castanet, J., Géraudie, J., Meunier, F.J., Sire, J.Y. et al. (1990) Microstructure and mineralization of vertebrate skeletal tissues. In: Carter, J.G. (Ed.) *Skeletal biomineralization: patterns, processes and evolutionary trends*, Vol. 1. New York, NY: Van Nostrand Reinhold, pp. 471–530.

Francillon-Vieillot, H., Meunier, F.J. & de Ricqles, A.N.D.A. (1993) Bone growth—B. In: Hall, B.K. (Ed.) *Bone*, Vol. 7. Boca Raton, FL: CRC Press, pp. 245–283.

Funston, G.F., Wilkinson, R.D., Simon, D.J., Leblanc, A.H., Wosik, M. & Currie, P.J. (2020) Histology of caenagnathid (Theropoda, Oviraptorosauria) dentaries and implications for development, ontogenetic edentulism, and taxonomy. *The Anatomical Record*, 303(4), 918–934.

Gao, C., Morschhauser, E.M., Varricchio, D.J., Liu, J. & Zhao, B. (2012) A second soundly sleeping dragon: new anatomical details of the Chinese troodontid *Mei long* with implications for phylogeny and taphonomy. *PLoS One*, 7(9), e45203.

Garros, C.W., Powers, M.J., Dyer, A.D., & Currie, P.J. (2022) Survey of metatarsal paleopathologies in coelurosauria from the Dinosaur Park Formation. *Journal of Vertebrate Paleontology, Program and Abstracts*, 156.

George, J.C. & Berger, A.J. (1966) *Avian myology*. New York & London: Academic Press.

Gianechini, F.A., Makovicky, P.J., Apesteguía, S. & Cerda, I. (2018) Postcranial skeletal anatomy of the holotype and referred specimens of *Buitreraptor gonzalezorum* Makovicky, Apesteguía and Agnolín 2005 (Theropoda, Dromaeosauridae), from the late cretaceous of Patagonia. *PeerJ*, 2018(3), e4558.

González, M.S. (2019) Skeletal bone structure and repair in small mammals, birds, and reptiles. *Veterinary Clinics: Exotic Animal Practice*, 22(2), 135–147. Available from: https://doi.org/10.1016/j.cvex.2019.01.002

Gonzalez, R., Gallina, P.A. & Cerda, I.A. (2017) Multiple paleopathologies in the dinosaur *Bonitasaura salgadoi* (Sauropoda: Titanosauria) from the upper cretaceous of Patagonia, Argentina. *Cretaceous Research*, 79, 159–170.

Griffin, C.T. (2018) Pathological bone tissue in a late Triassic neotheropod fibula, with implications for the interpretation of medullary bone. *New Jersey State Museum Investigations*, 6, 2–10.

Grosso, F.V. (2019) Orthopedic diagnostic imaging in exotic pets. *Veterinary Clinics: Exotic Animal Practice*, 22(2), 149–173. Available from: https://doi.org/10.1016/j.cvex.2019.01.003

Hammer, Ø. & Harper, D.A. (2001) Past: paleontological statistics software package for educaton and data anlysis. *Palaeontologia Electronica*, 4(1), 1.

Hartman, S., Mortimer, M., Wahl, W.R., Lomax, D.R., Lippincott, J. & Lovelace, D.M. (2019) A new paravian dinosaur from the late Jurassic of North America supports a late acquisition of avian flight. *PeerJ*, 7, e7247.

Hartup, B.K., Lauer, S.J. & Manthei, A.R. (2018) Osteoarthritis in the pelvic limb of captive cranes. *Proceedings of the North American Crane Workshop*, 14(2018), 145–148.

Hernandez-Divers, S.M. & Garner, M.M. (2003) Neoplasia of reptiles with an emphasis on lizards. *Veterinary Clinics: Exotic Animal Practice*, 6(1), 251–273. Available from: https://doi.org/10.1016/s1094-9194(02)00028-2

Holtz, T.R., Jr. (1995) The arctometatarsalian pes, an unusual structure of the metatarsus of cretaceous Theropoda (Dinosauria: Saurischia). *Journal of Vertebrate Paleontology*, 14(4), 480–519.

Horner, J.R., Padian, K. & de Ricqlès, A. (2001) Comparative osteohistology of some embryonic and perinatal archosaurs: developmental and behavioral implications for dinosaurs. *Paleobiology*, 27(1), 39–58.

Huchzermeyer, F.W. & Cooper, J.E. (2000) Fibriscess, not abscess, resulting from a localised inflammatory response to infection in reptiles and birds. *Veterinary Record*, 147(18), 515–516.

Hutchinson, J.R. (2002) The evolution of hindlimb tendons and muscles on the line to crown-group birds. *Comparative Biochemistry and Physiology Part A: Molecular & Integrative Physiology*, 133(4), 1051–1086.

Huttenlocker, A.K., Woodward, H.N. & Hall, B.K. (2013) The biology of bone. In: Padian, K. & Lamm, E.T. (Eds.) *Bone histology of fossil tetrapods: advancing methods, analysis, and interpretation*. Berkley, CA: University of California Press, pp. 13–34.

Hutton, J.M. (1986) Age determination of living Nile crocodiles from the cortical stratification of bone. *Copeia*, 1986, 332–341.

Jin, X., Varricchio, D.J., Poust, A.W. & He, T. (2019) An oviraptorosaur adult-egg association from the cretaceous of Jiangxi Province, China. *Journal of Vertebrate Paleontology*, 39(6), e1739060. Available from: https://doi.org/10.1080/02724634.2019.1739060

Kato, K.M., Rega, E.A., Sidor, C.A. & Huttenlocker, A.K. (2020) Investigation of a bone lesion in a gorgonopsian (Synapsida) from the Permian of Zambia and periosteal reactions in fossil non-mammalian tetrapods. *Philosophical Transactions of the Royal Society B*, 375(1793), 20190144.

Kealy, J.K., McAllister, H. & Graham, J.P. (2011) Chapter four – Bones and joints. In: Kealy, J.K., McAllister, H. & Graham, J.P. (Eds.) *Diagnostic radiology and ultrasonography of the dog and cat*, 5th edition. Philadelphia, PA: W.B. Saunders, pp. 351–446.

Krautwald-Junghanns, M.E. & Schmidt, V. (2011) Birds. Special diagnostics, pathological findings. Skeletal system. In: Krautwald-Junghanns, M.E., Pees, M. & Reese, S. (Eds.) *Diagnostic imaging of exotic pets. Birds-small mammals-reptiles*. Hannover: Schlütersche, 70–53.

Kuehn, A.L., Lee, A.H., Main, R.P. & Simons, E.L.R. (2019) The effects of growth rate and biomechanical loading on bone laminarity within the emu skeleton. *PeerJ*, 7, e7616.

Lee, A.H. & O'Connor, P.M. (2013) Bone histology confirms determinate growth and small body size in the noasaurid theropod *Masiakasaurus knopfleri*. *Journal of Vertebrate Paleontology*, 33(4), 865–876. Available from: https://doi.org/10.1080/02724634.2013.743898

Lee, S.H. & Yun, S.J. (2017) Iliac subperiosteal hematoma with ossification in a 15-year-old boy. *The Journal of Pediatrics*, 190, 285.e1.

Li, G., Yin, J., Gao, J., Cheng, T.S., Pavlos, N.J., Zhang, C. et al. (2013) Subchondral bone in osteoarthritis: insight into risk factors and microstructural changes. *Arthritis Research & Therapy*, 15, 1–12.

Lieberman, D.E., Pearson, O.M., Polk, J.D., Demes, B. & Crompton, A.W. (2003) Optimization of bone growth and remodeling in response to loading in tapered mammalian limbs. *Journal of Experimental Biology*, 206(18), 3125–3138.

Lü, J., Xu, L., Liu, Y., Zhang, X., Jia, S., & Ji, Q. (2012) A new troodontid theropod from the late cretaceous of central China, and the radiation of asian troodontids. *Acta Palaeontologica Polonica*, 55(3), 381–388. Available from: https://doi.org/10.4202/app.2009.0047

Main, R.P., Simons, E.L. & Lee, A.H. (2021) Interpreting mechanical function in extant and fossil long bones. In: de Buffrénil, V., de Ricqlès, A.J., Zylberberg, L. & Padian, K. (Eds.) *Vertebrate skeletal histology and paleohistology*. Boca Raton, FL: CRC Press, pp. 688–723.

Majithia, V. & Geraci, S.A. (2007) Rheumatoid arthritis: diagnosis and management. *The American Journal of Medicine*, 120(11), 936–939.

Martin, D., Caizhi, S. & Kundrát, M. (2023) Intraindividual variability of the histological, chronological and growth patterns in postcranial elements of *Liaoningvenator curriei* (Paraves: Troodontidae). *Historical Biology*, 36(3), 1–21.

Martin, D., Currie, P.J. & Kundrát, M. (2024) Variability of bone microstructure and growth lines in the evolution of troodontids and dromaeosaurids. *Acta Zoologica*, 105(2), 135–175.

Martin, R.B. (2002) Is all cortical bone remodeling initiated by microdamage? *Bone*, 30(1), 8–13.

Munger, A.M., Lindskog, D.M. & Gardner, E.C. (2021) Case report: Ossified subperiosteal hematoma in the humerus of a lacrosse player. *International Journal of Sports and Exercise Medicine*, 7(6), 208–210. Available from: https://doi.org/10.23937/2469-5718/1510208

Norell, M.A., Makovicky, P.J., Bever, G.S., Balanoff, A.M., Clark, J.M., Barsbold, R. et al. (2009) A review of the Mongolian cretaceous dinosaur *Saurornithoides* (Troodontidae: Theropoda). *American Museum Novitates*, 2009(3654), 1–63.

Padian, K. & Lamm, E.T. (Eds.). (2013) *Bone histology of fossil tetrapods: advancing methods, analysis, and interpretation*. Berkeley CA: University of California Press.

Palmer, N. (1992) Bones and joints. In: Jubb, K.V.F., Kennedy, P.C. & Palmer, N. (Eds.) *Pathology of domestic animals*, Vol. 1, 4th edition. San Diego, CA: Academic Press, Inc, pp. 1–181.

Patak, A. & Baldwin, J. (1993) Structural and metabolic characterization of the muscles used to power running in the emu (*Dromaius novaehollandiae*), a giant flightless bird. *Journal of Experimental Biology*, 175(1), 233–249.

Persons, W.S., IV & Currie, P.J. (2016) An approach to scoring cursorial limb proportions in carnivorous dinosaurs and an attempt to account for allometry. *Scientific Reports*, 6(1), 19828.

Prondvai, E., Godefroit, P., Adriaens, D. & Hu, D.Y. (2018) Intraskeletal histovariability, allometric growth patterns, and their functional implications in bird-like dinosaurs. *Scientific Reports*, 8(1), 258.

Prondvai, E., Stein, K.H., De Ricqlès, A. & Cubo, J. (2014) Development-based revision of bone tissue classification: the importance of semantics for science. *Biological Journal of the Linnean Society*, 112(4), 799–816. Available from: https://doi.org/10.1111/bij.12323

Rajapakse, B.N. & Kiddle, G. (2006) Calcifying haematoma mimicking a soft tissue sarcoma and myositis ossificans. *ANZ Journal of Surgery*, 76(11), 1027–1029.

Rhodes, M.M., Henderson, D.M. & Currie, P.J. (2021) Maniraptoran pelvic musculature highlights evolutionary patterns in theropod locomotion on the line to birds. *PeerJ*, 9, e10855.

Ricklefs, R.E. (1968) Patterns of growth in birds. *Ibis*, 110(4), 419–451.

Rothschild, B. (2009) Scientifically rigorous reptile and amphibian osseous pathology: lessons for forensic herpetology from comparative and paleo-pathology. *Applied Herpetology*, 6(1), 47–79.

Rothschild, B. (2010) Macroscopic recognition of nontraumatic osseous pathology in the postcranial skeletons of crocodilians and lizards. *Journal of Herpetology*, 44(1), 13–20.

Rothschild, B. & Lambert, H.W. (2021) First documentation of a greenstick fracture in the fossil record. possible gout also noted in *Arkansaurus fridayii*. *Historical Biology*, 33(9), 1349–1351. Available from: https://doi.org/10.1080/08912963.2019.1693558

Rothschild, B.M. (1990) Radiologic assessment of osteoarthritis in dinosaurs. *Annals of Carnegie Museum*, 59(4), 295–301.

Russell, D.A. (1969) A new specimen of *Stenonychosaurus* from the Oldman formation (cretaceous) of Alberta. *Canadian Journal of Earth Sciences*, 6(4), 595–612. Available from: https://doi.org/10.1139/e69-059

Russell, D.A. & Séguin, R. (1982) Reconstructions of the small cretaceous theropod *Stenonychosaurus inequalis* and a hypothetical dinosauroid. *Syllogeus*, 37, 1–43.

Sellés, A.G., Vila, B., Brusatte, S.L., Currie, P.J. & Galobart, À. (2021) A fast-growing basal troodontid (Dinosauria: Theropoda) from the latest cretaceous of Europe. *Scientific Reports*, 11(1), 4855.

Senter, P. & Juengst, S.L. (2016) Record-breaking pain: the largest number and variety of forelimb bone maladies in a theropod dinosaur. *PLoS One*, 11(2), e0149140.

Shen, C., Lü, J., Gao, C., Hoshino, M., Uesugi, K. & Kundrát, M. (2017) Forearm bone histology of the small theropod *Daliansaurus liaoningensis* (Paraves: Troodontidae) from the Yixian formation, Liaoning, China. *Historical Biology*, 31(2), 253–261. Available from: https://doi.org/10.1080/08912963.2017.1360296

Shen, C., Zhao, B., Gao, C., Lü, J. & Kundrát, M. (2017) A new troodontid dinosaur (*Liaoningvenator curriei* gen. Et sp. nov.) from the early cretaceous Yixian formation of Western Liaoning Province, China. *Acta Geoscientica Sinica*, 38(3), 1–13.

Shine, R. & Charnov, E.L. (1992) Patterns of survival, growth, and maturation in snakes and lizards. *The American Naturalist*, 139(6), 1257–1269.

Sokoloff, L. (1959) Osteoarthritis in laboratory animals. *Laboratory Investigation; a Journal of Technical Methods and Pathology*, 8, 1209–1217.

Stacy, B.A. & Pessier, A.P. (2007) Host response to infectious agents and identification of pathogens in tissue sections. In: Jacobson, E.R. (Ed.) *Infectious diseases and pathology of reptiles*. Boca Raton, FL: CRC Press, pp. 257–297.

Sternberg, C.M. (1932) Two new theropod dinosaurs from the Belly River formation of Alberta. *Canadian Field-Naturalist*, 46, 99–105.

Straight, W.H., Davis, G.L., Skinner, H.C.W., Haims, A., McClennan, B.L. & Tanke, D.H. (2009) Bone lesions in hadrosaurs: computed tomographic imaging as a guide for paleohistologic and stable-isotopic analysis. *Journal of Vertebrate Paleontology*, 29(2), 315–325.

Tanke, D.H. & Rothschild, B.M. (2002) *Dinosores: an annotated bibliography of dinosaur paleopathology and related topics—1838–2001: bulletin 20*, Vol. 20. Albuquerque, NM: New Mexico Museum of Natural History and Science.

Tschopp, E., Wings, O., Frauenfelder, T. & Rothschild, B.M. (2014) Pathological phalanges in a camarasaurid sauropod dinosaur and implications on behaviour. *Acta Palaeontologica Polonica*, 61(1), 125–134. Available from: https://doi.org/10.4202/app.00119.2014

Tsogtbaatar, C., Beguesse, K.A., Canoville, A., Phillips, G. & Zanno, L.E. (2023) Chronic fracture and osteomyelitis in a large-bodied ornithomimosaur with implications for the identification of unusual endosteal bone in the fossil record. *The Anatomical Record*, 306(7), 1864–1879. Available from: https://doi.org/10.1002/ar.25069

Tsuihiji, T., Barsbold, R., Watabe, M., Tsogtbaatar, K., Chinzorig, T., Fujiyama, Y. et al. (2014) An exquisitely preserved troodontid theropod with new information on the palatal structure from the upper cretaceous of Mongolia. *Naturwissenschaften*, 101, 131–142.

Tütken, T., Pfretzschner, H.U., Vennemann, T.W., Sun, G. & Wang, Y.D. (2004) Paleobiology and skeletochronology of Jurassic dinosaurs: implications from the histology and oxygen isotope compositions of bones. *Palaeogeography, Palaeoclimatology, Palaeoecology*, 206(3–4), 217–238.

van der Reest, A.J. & Currie, P.J. (2017) Troodontids (Theropoda) from the Dinosaur Park formation, Alberta, with a description of a unique new taxon: implications for deinonychosaur diversity in North America. *Canadian Journal of Earth Sciences*, 54(9), 919–935.

Varricchio, D.J. (1993) Bone microstructure of the upper cretaceous theropod dinosaur *Troodon formosus*. *Journal of Vertebrate Paleontology*, 13(1), 99–104. Available from: https://doi.org/10.1080/02724634.1993.10011490

Varricchio, D.J., Moore, J.R., Erickson, G.M., Norell, M.A., Jackson, F.D. & Borkowski, J.J. (2008) Avian paternal care had dinosaur origin. *Science*, 322(5909), 1826–1828.

Wainwright, S.A. (1982) *Mechanical design in organisms*. Princeton, NJ: Princeton University Press.

Wang, S., Zhang, Q., Tan, Q., Jiangzuo, Q., Zhang, H. & Tan, L. (2022) New troodontid theropod specimen from Inner Mongolia, China clarifies phylogenetic relationships of later-diverging small-bodied troodontids and paravian body size evolution. *Cladistics*, 38(1), 59–82.

Williams, J. (2002) Orthopedic radiography in exotic animal practice. *The Veterinary Clinics of North America. Exotic Animal Practice*, 5(1), 1–22. Available from: https://doi.org/10.1016/s1094-9194(03)00043-4

Wilson, M.C. & Currie, P.J. (1985) *Stenonychosaurus inequalis* (Saurischia: Theropoda) from the Judith River (Oldman) formation of Alberta: new findings on metatarsal structure. *Canadian Journal of Earth Sciences*, 22, 1813–1817.

Xing, L., Niu, K., Lockley, M.G., Romilio, A., Deng, K. & Persons, W.S. (2024) Deinonychosaur trackways in southeastern China record a possible giant troodontid. *iScience*, 27(5), 109598. Available from: https://doi.org/10.1016/j.isci.2024.109598

Xu, X. & Norell, M.A. (2004) A new troodontid dinosaur from China with avian-like sleeping posture. *Nature*, 431(7010), 838–841.

Xu, X., Zhao, Q., Norell, M., Sullivan, C., Hone, D., Erickson, G. et al. (2008) A new feathered maniraptoran dinosaur fossil that fills a morphological gap in avian origin. *Chinese Science Bulletin*, 54(3), 430–435. Available from: https://doi.org/10.1007/s11434-009-0009-6

Xu, X., Zhao, Q., Sullivan, C., Tan, Q.W., Sander, M. & Ma, Q.Y. (2012) The taxonomy of the troodontid IVPP V 10597 reconsidered. *Vertebrata Palasiatica*, 50(2), 140–150.

Zanno, L.E., Varricchio, D.J., O'Connor, P.M., Titus, A.L. & Knell, M.J. (2011) A new troodontid theropod, *Talos sampsoni* gen. Et sp. nov., from the upper cretaceous Western Interior Basin of North America. *PLoS One*, 6(9), e24487.

SUPPORTING INFORMATION

Additional supporting information can be found online in the Supporting Information section at the end of this article.

How to cite this article: Garros, C.W., Powers, M.J., Dyer, A.D. & Currie, P.J. (2025) Osteohistological analysis of metatarsals reveals new information on pathology and life history of troodontids from the Campanian Dinosaur Park Formation, Alberta, Canada. *Journal of Anatomy*, 00, 1–29. Available from: https://doi.org/10.1111/joa.14262